Fault relay zones evolving through distributed longitudinal fractures: The case of the Teruel graben system (Iberian Chain, Spain)

Alba Peiro* apeiro@unizar.es, José Luis Simón jsimon@unizar.es, Teresa Román-Berdiel mtdjrb@unizar.es

Dpto. de Ciencias de la Tierra, Grupo Geotransfer - Instituto Universitario de Investigación en Ciencias Ambientales de Aragón (IUCA), Universidad de Zaragoza, Pedro Cerbuna 12, 50009, Zaragoza, Spain

*Corresponding author.

Abstract

A new type of fault relay zone in extensional contexts, dominated by distributed along-strike or longitudinal fractures, is defined. It contrasts with the classical models reported in the literature, in which transverse connecting faults controlled by the own relay kinematics prevail. The new model is based on structural features of the Teruel graben system, as well as on analogue modelling. Relay zones between the NW-SE to NNW-SSE striking faults that delimit the eastern boundary of the Jiloca Graben (Calamocha, Sierra Palomera and Concud faults), together with the Teruel Fault, have been studied. All of these relay faults show recent (Neogene-Quaternary) ruptures at different scales, mostly parallel to the macrostructural trend and to the maximum horizontal stress (S_{Hmax}) trajectories (i.e., orthogonal to the ENE-WSW regional extension direction that characterises the nearly biaxial or radial stress regime active during Upper Pliocene-Quaternary times). Transverse ruptures are almost absent, with the exception of the northern relay zone (Calamocha-Sierra Palomera), where an incipient NE-SW striking connecting fault does exist. Analogue models have been run under a biaxial extension regime similar to the regional one. They allowed analysing the main factors controlling fracture propagation, depending on the ratio of extension velocities and the orientation of the master faults relative to extension directions. Laboratory fracture patterns, as in the natural studied examples, are mostly controlled by the inherited anisotropies and, in a greater extent, by the imposed extension trajectories, which results in a clear prevalence of longitudinal fractures. Such external controls, usually disregarded in numerical and analogue modelling, tend to

induce fault coalescence through along-strike (parallel or at very-low-angle) propagation resulting in a final braided fault pattern.

Keywords: Fault interaction; Jiloca graben; Along-strike propagation; Biaxial extension; Analogue modelling

1 Introduction

Fault relay zones within extensional settings have been widely studied (e.g., Peacock and Sanderson, 1994; Childs et al., 1995; Willemse, 1997; Crider and Pollard, 1998; Peacock, 2002; Fossen and Rotevatn, 2016). Many publications reveal increasing interest on relationships between fault relay zones and oil or gas reservoirs (Fossen et al., 2005; Rotevatn et al., 2007), as well as on their behaviour during seismic events (Machette et al., 1991; Manighetti et al., 2009; Finzi and Langer, 2012). Models of fault linkage controlled by fault interaction and propagation, based on numerical and analogue modelling as well as on natural examples, have been extensively developed. The basic evolutionary model from two non-interacting overstepping segments to a single fault includes development of a relay ramp (*soft linkage*) followed by a breached ramp stage (*hard linkage*) (e.g. Walsh and Watterson, 1991; Peacock and Sanderson, 1994; Young et al., 2001; Fossen and Rotevatn, 2016). Concerning hard linkage, this could have been achieved through full connecting faults, or lie in a transient, incomplete stage (*incipient hard linkage*). Those evolutionary stages can be related to characteristic displacement-length profiles that express the degree and type of fault interaction prior to linkage (Peacock and Sanderson, 1991; Cartwrigth et al., 1995; Gawthorpe and Leeder, 2000; Mansfield and Cartwright, 2001).

Most published pictures and sketches that represent the conceptual model of a breached relay zone show secondary faults at high angles (>45-50°) to the master faults (Fig. 1A,B,C,D; Ramsay and Huber, 1987, p. 533; Peacock and Sanderson, 1994, [Instruction: Within the introduction section, there are two types of references to Figures:
a) References to Figure 1A,B,C,D,E,F,G,H,I,J, which is the one included in this paper and should be properly linked with Fig. 1. These references where originally written in capital letter, for example: Fig.1A,B,C,D.
b) References to figures not included in this paper but belonging to papers cited in this section. They were originally written in small letter and always follow their corresponding references, and they should not be linked with Figures from the present paper. So, in our opinion, these capital letters should be rewritten in small letters. The correct version is for example: Peacock and Sanderson, 1994, figs 1, 3d, 12.
]Figs. 1, 3d and 12; Ferrill and Morris, 2001, Fig. 8d; Peacock, 2002, Fig. 3c; Fossen and Rotevatn, 2016). Such conceptual model obeys the notion that breaching occurs at a given level of bending curvature at the relay ramp, owing to lengthening of material parallel to the master faults (Fossen and Rotevatn, 2016). Nevertheless, comparatively few works describe actual visible examples of such transverse connecting faults (e.g. Peacock and Sanderson, 1994, Figs. 2, 14 and 15; Young et al., 2001). We set aside the case of nearly vertical, dominantly strike-slip faults that transfer displacement between two adjacent fault zones with differential extension rate (transfer faults s.s.; Gibbs, 1984, 1990), which in our opinion should not be

assimilated to *hard linkage* as some authors implicitly do (e.g. Gawthorpe and Hurst, 1993; Acocella et al., 2005).

alt-text: Fig. 1

Fig. 1

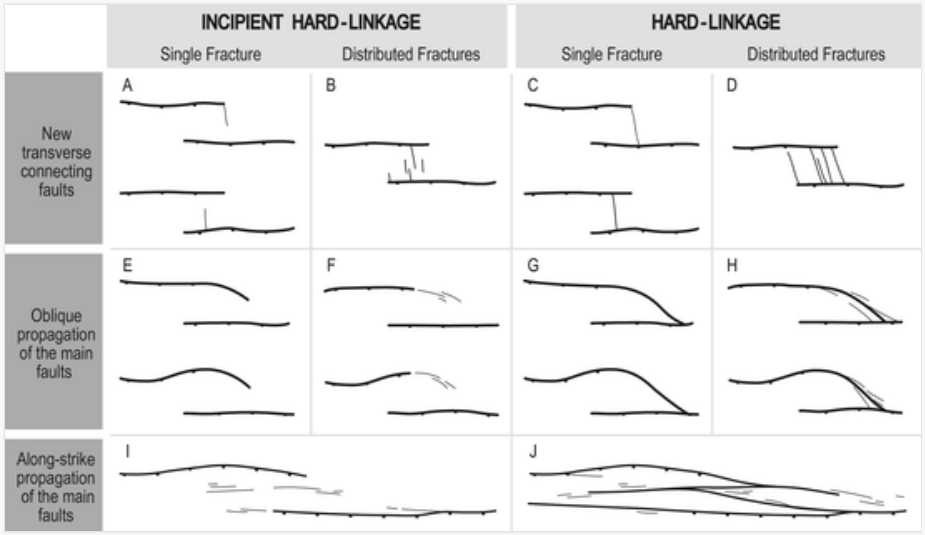

Classification of fracture patterns within fault relay zones in extensional contexts based on literature reviewing. A, B, C, D: e.g., Ramsay and Huber (1987), p. 533; Peacock and Sanderson (1994), Figs. 1, 3d and 12; Ferrill and Morris, 2001, Fig. 8d; Peacock (2002), Fig. 3c; Fossen and Rotevatn (2016). E, G: e.g., Peacock and Sanderson (1994), Fig. 7a and b; Childs et al. (1995), Fig. 12 ; Walsh et al. (1999), Fig. 3d; Peacock (2002), Fig. 1b; Le Calvez and Vendeville (2002), Fig. 15; Moustafa and Khalil (2016), Fig. 12. F, H: e.g., Peacock and Sanderson (1994), Fig. 2; Gupta and Scholz (2000), Fig. 2. I, J: e.g., Peacock and Sanderson (1994), Figs. 4a, 9a and 16a; Trudgill and Cartwright (1994), Figs. 3b, 5 and 6; Childs et al. (1995); Huggins et al. (1995); Crider and Pollard (1998); Walsh et al. (1999), Figs. 3d and 5a; Morley and Wonganan (2000); Mansfield and Cartwright (2001), Fig. 7; Nicol et al. (2005), Fig. 3; Fossen and Rotevatn (2016), Figs. 3a and 6; Moustafa and Khalil (2016); Fig. 9.

alt-text: Fig. 2

Fig. 2

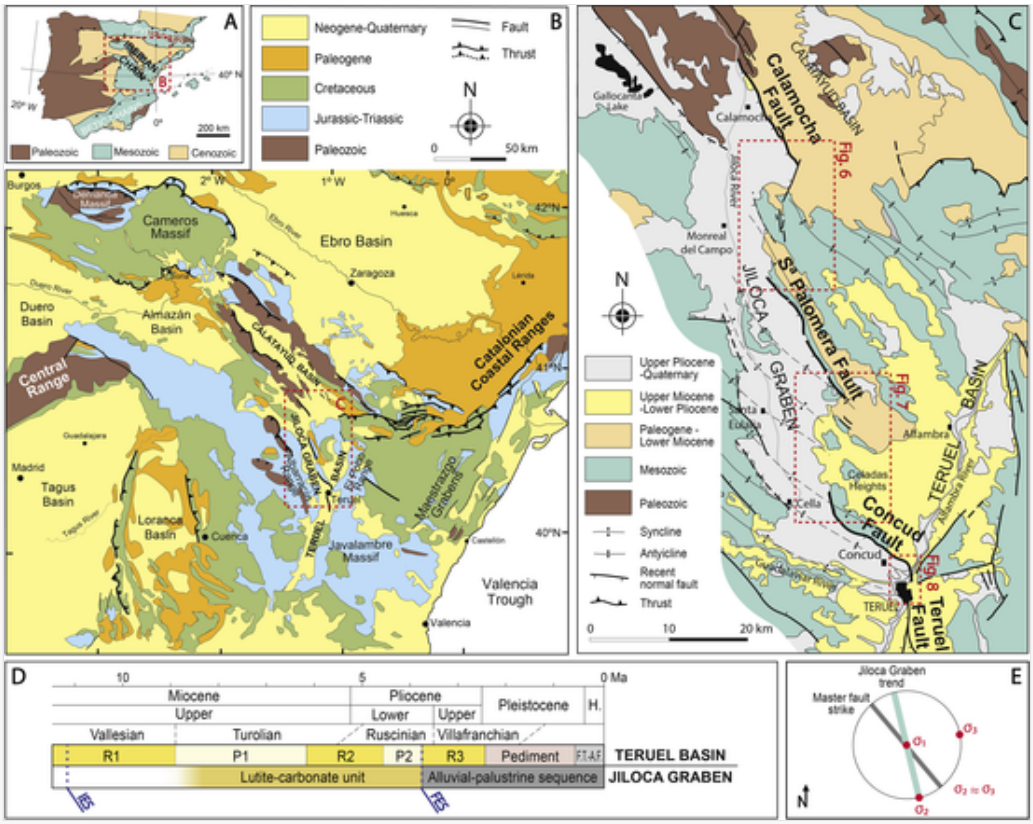

(A) Location of the Iberian Chain within the Iberian Peninsula. (B) Location of the Teruel graben system within the Iberian Chain. (C) Geological map of the Teruel graben system, with location of Figs. 6–8. (D) Chronostratigraphical diagram of sedimentary units of the Teruel (R1: Rojo 1 unit; P1: Páramo 1; R2: Rojo 2; P2: Páramo 2; R3: Rojo 3; F.T.-A.F. fluvial terraces and alluvial fans) and Jiloca basins, showing the position of the Intramiocene Erosion Surface (IES) and Fundamental Erosion Surface (FES). (E) Sketch of structural trends and their relationship with regional stress directions.

alt-text: Fig. 3

Fig. 3

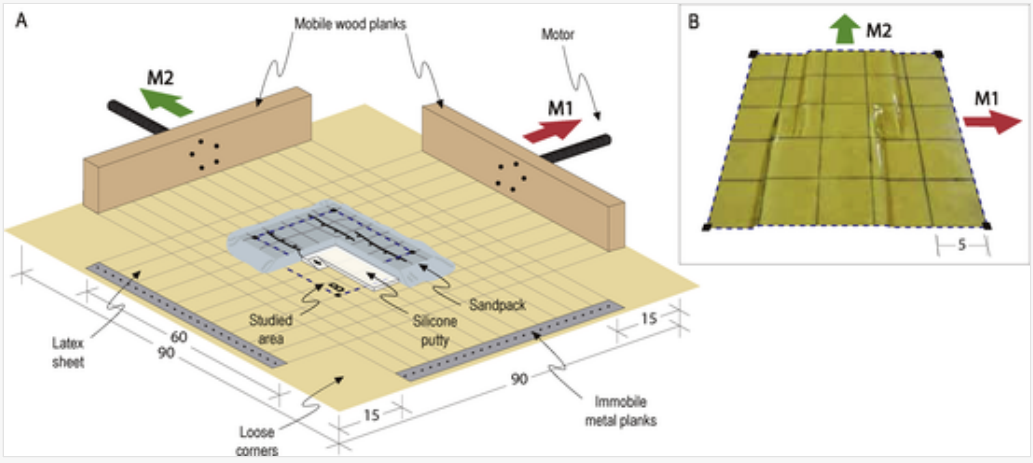

(A) Experimental set-up. (B) Detail of the studied area and the silicone strip configuration in models B1-1 and B[Instruction: In our opinion, the distribution of figures along the layout version of the paper is not the most adequate. Many figures appear quite far from the related text. After this comment and in several ones along this document, we propose a number of changes in order to

improve such correspondence between figures and text. At the same time, we include other proposals relative to size of figures, with the aim of making it more homogeneous in the case of figures that express similar things.

Fig. 3 on the PDF version could be placed in the next page, separately from Fig. 2 and closer to Figs. 4 and 5. This would allow to place the paragraphs from the geological setting closer to Fig. 2.]2-1.

Indeed, as illustrated in literature, relay zones in both nature and laboratory experiments show a wide variety of faulting geometries that do not fit that conceptual model. In contrast with the scarce above-mentioned cases of high-angle connecting faults (Peacock and Sanderson, 1994; Young et al., 2001), low-angle oblique faults (usually in the range of 20-40° to the major faults) are very frequent in relay zones, either as single ruptures propagated from one of the fault tips (Fig. 1E,G; e.g., Peacock and Sanderson, 1994, Fig. 7a,b; Childs et al., 1995, Fig. 12; Walsh et al., 1999, Fig. 3d; Peacock, 2002, Fig. 1b; Le Calvez and Vendeville, 2002, Fig. 15; Moustafa and Khalil, 2016, Fig. 12), or as distributed ruptures (Fig. 1F,H; e.g., Peacock and Sanderson, 1994, Fig. 2; Gupta and Scholz, 2000, Fig. 2). Fracture patterns nearly parallel, <20° to the major faults, are also frequent (Fig. 1I and J): (i) along-strike faults or fault zones propagated from a major fault tip, which can abut the second major fault without any significant deviation since its incidence angle lies within the strike variability (Peacock and Sanderson, 1994, Fig. 16a; Childs et al., 1995; Crider and Pollard, 1998; Walsh et al., 1999, Figs. 3d and 5a; Nicol et al., 2005, Fig. 3; Fossen and Rotevatn, 2016, Fig. 6); (ii) longitudinal distributed fracture patterns that randomly extend within and near the relay zone, frequently including both synthetic and antithetic faults (Huggins et al., 1995; Peacock and Sanderson, 1994, Figs. 4a and 9a; Trudgill and Cartwright, 1994, Figs. 3b, 5 and 6; Morley and Wonganan, 2000; Mansfield and Cartwright, 2001, Fig. 7; Moustafa and Khalil, 2016, Fig. 9; Fossen and Rotevatn, 2016, Fig. 3a). Finally, multiple fracture sets derived from inherited structures can also develop (e.g. Trudgill and Cartwright, 1994, Fig. 3b; Fossen and Rotevatn, 2016), eventually giving rise to zigzag basin margins after full linkage (e.g., Younes and McClay, 2002; Gawthorpe et al., 2003; Moustafa and Khalil, 2016).

alt-text: Fig. 4

Fig. 4

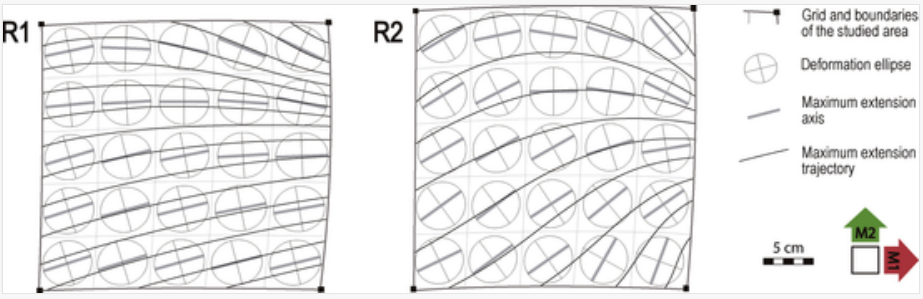

Reference models R1 and R2 defining the strain field imposed in models of Series 1 and 2, respectively. Extension trajectories inferred from latex sheet deformation, then transferred to the sand pack, are shown.

alt-text: Fig. 5

Fig. 5

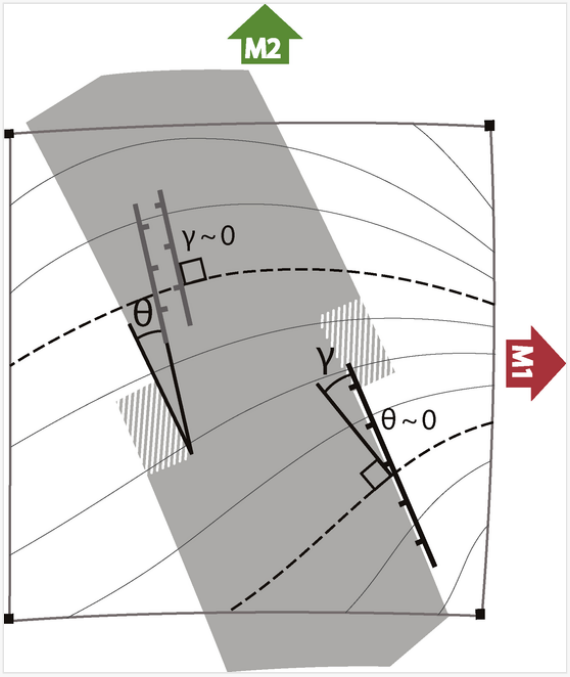

Angles used for detailed analysis of fractures developed in analogue models; γ: angle between an individual fracture segment and the normal to the extension trajectory; θ: angle between an individual fracture segment and the orientation of the silicone [Instruction: Size of models in Figs. 4, 5, 9 and 10 should be as similar as possible to each other on the PDF version. The size of the studied area in Fig. 5 is too large, while in Fig. 10 is too small. Fig. 5 should be reduced up to approach the size of each square sketch in Fig. 4 (although they need not to be exactly equal in size). In the same way, while Fig. 9 can remain in its present size, enlarging Fig. 10 up to the box width would allow approaching their respective sizes.
]strip.

alt-text: Fig. 6

Fig. 6

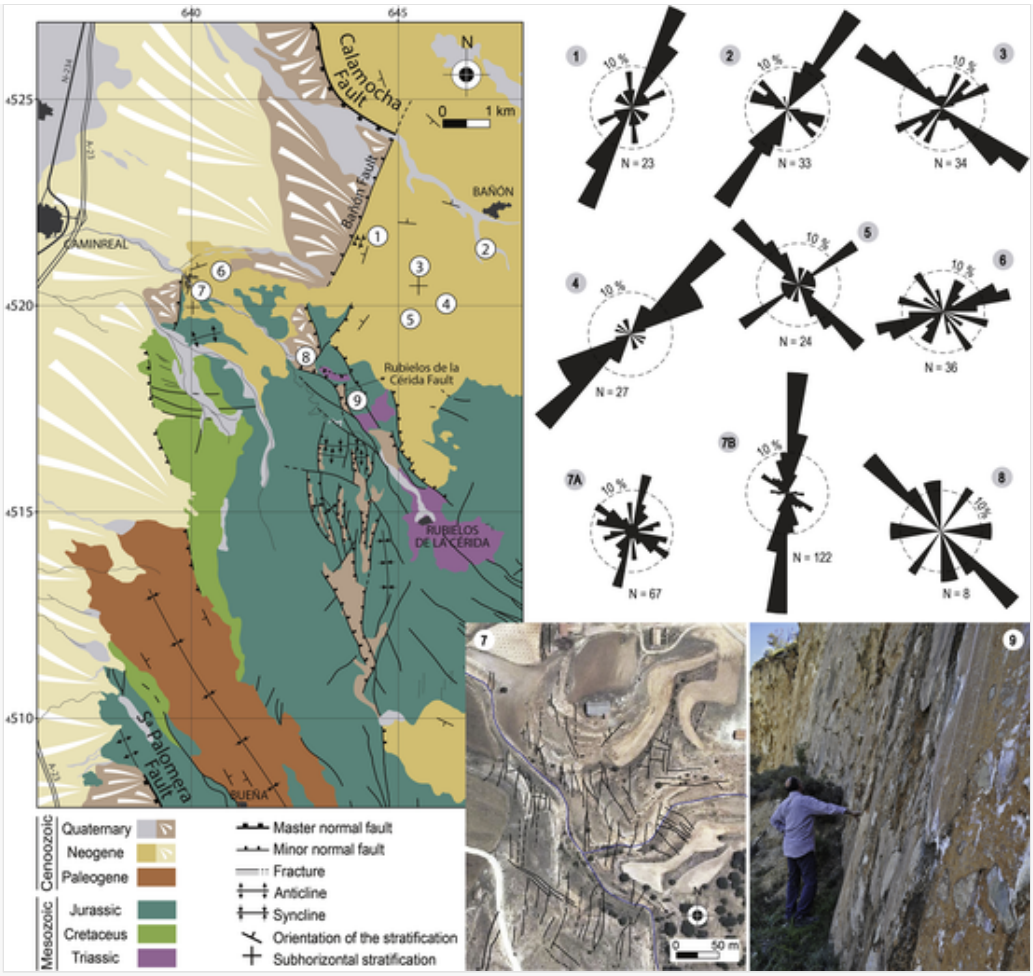

Geological map and fracture patterns of the northern relay zone, between the Calamocha and Sierra Palomera (see location in Fig. 2B). Rose diagrams show strike distributions of mesostructural fractures measured in sites 1–8; in the case of site 7, fractures and faults are distinguished (7A and 7B, respectively). 7C: detailed fracture map of Site 7.9: Outcrop of the Rubielos de la Cérida [Instruction: Figs. 6, 7 and 8 on the PDF version should be placed within Section “5. Fracture patterns within fault relay zones", where the reader will find their references. Pages before this section would consist in text, filling completely the corresponding pages (with sections 2, 3 and 4), without figures.
]Fault.

alt-text: Fig. 7

Fig. 7

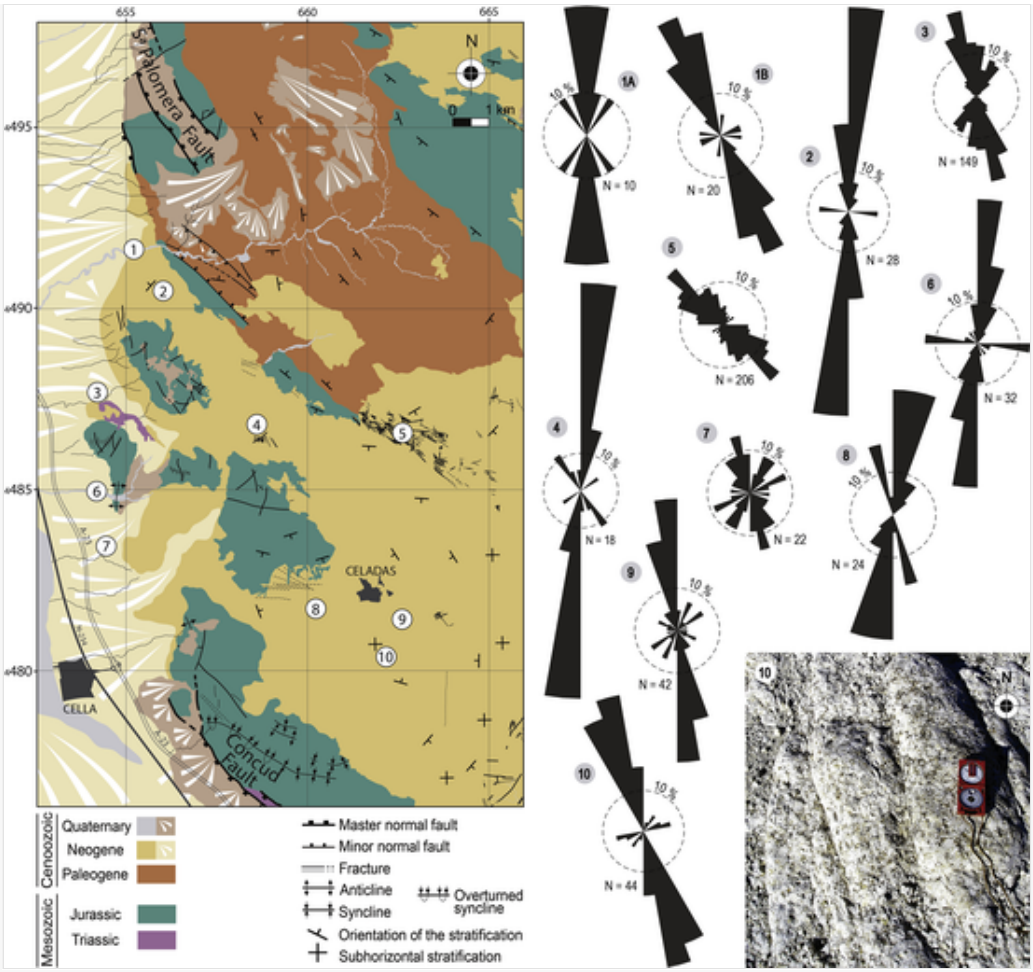

Geological map and fracture patterns of the central relay zone, between the Sierra Palomera and Concud faults (see location in Fig. 2B). Rose diagrams show strike distributions of mesostructural fractures measured in sites 1–10; for site 1, fractures in units from the Upper Pliocene and the Villafranchian pediment are distinguished (1A and 1B, respectively). Photo 10: field view of systematic NNW-SSE striking fractures cutting Miocene limestones in Site 1[Instruction: Figs. 6 and 7 seem to have been a bit darken during the process ¿Could this be fixed? Please, find attached an example of the original Fig. 7 (left side of the picture) and the one in the proof (right side of the picture)
]0.

alt-text: Fig. 8

Fig. 8

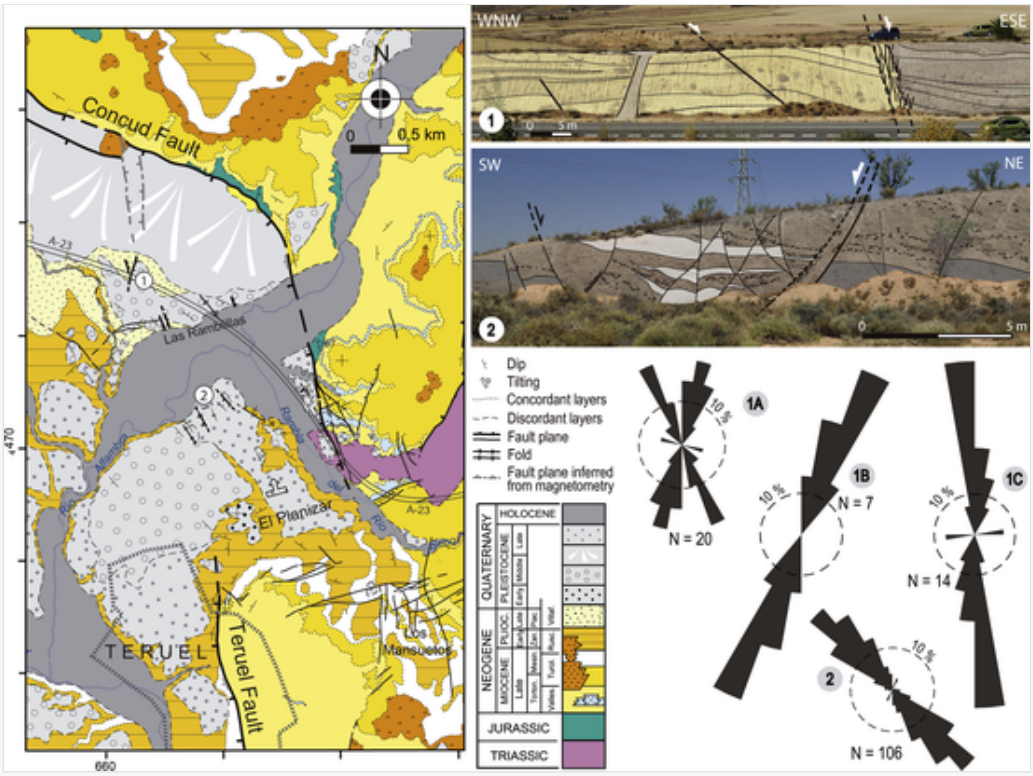

Geological map and fracture patterns of the southern relay zone, between the Concud and Teruel faults (map modified from Lafuente et al., 2011; see location in Fig. 2B). Rose diagrams show strike distributions of mesostructural fractures measured in sites 1 and 2, whose overall field views are shown in 1A and 2A, respectively. For site 1, fractures in the footwall block, main fault zone and hanging-wall block are distinguished (diagrams 1A, 1B and 1C, respectively).

alt-text: Fig. 9

Fig. 9

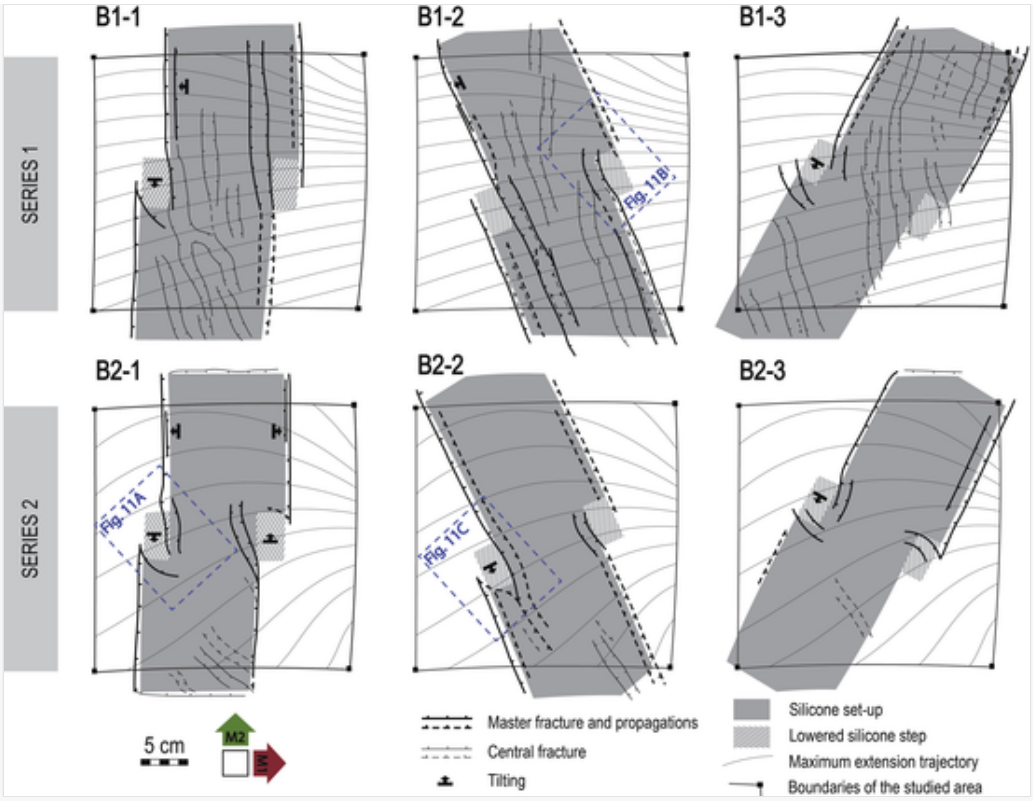

Line drawing of surface fracture patterns developed in models of Series 1 (B1-1, B1-2 and B1-3) and Series 2 (B2-1, B2-2 and B2-3), with location of Fig. 11A, B and 1[Instruction: Fig. 9 on the PDF version could be placed within or next to Section "6. Experimental results", where the reader will find their references (and hence closer to Fig. 10).
]1C.

Fig. 1 compiles such diverse typology of fracture patterns associated to fault relay zones, considering: (i) the angle of the newly propagating ruptures with respect to the master faults (high-angle or transverse, low-angle oblique, and very-low-angle or along-strike propagating ruptures are distinguished); (ii) cases of complete breaching (*hard linkage*) vs. incomplete breaching (*incipient hard linkage*); (iii) cases where deformation is accommodated on a single fault and others where it is distributed among several ruptures. We should pay special attention to along-strike propagated ruptures in relay zones (Fig. 1I and J), as most actual fault zones show an anastomosing geometry made of distinct traces oriented at very-low-angles to each other. They likely developed from initially relay-arranged individual segments, which should coalesce into a merged fault zone without mediation of any high-angle, transverse connecting fault.

Most conceptual, analogue and numerical models initially consider (i) a non-deformed rock body in which new fault systems develop, and (ii) just kinematic boundary conditions (velocities and displacements), so that reciprocal interaction between master faults and secondary fractures is only subject to such kinematic constraints (e.g. Childs et al., 1993; Gupta and Scholz, 2000; Ferrill and Morris, 2001). However, extensional faulting (i) frequently develops in areas with inherited faults and fractures, and (ii) is controlled by the coeval regional and local stress fields. The influence of structural inheritance and dynamical boundary conditions on fracture propagation within fault relay zones has not received enough attention in the literature.

The purpose of the present work is to provide insight into the genetic conditions in which other structural patterns, different from transverse connecting faults typically identified with *hard linkage*, can develop. Our analysis is based upon both field examples and analogue models, controlled, in both cases, by an extensional stress regime. First, we describe and analyse fracture patterns within relay zones between major faults of the Teruel graben system (Jiloca and Teruel basins), active during Upper Pliocene-Quaternary times under a nearly biaxial or radial extensional stress field (maximum principal stress σ_1 vertical; $\sigma_2 \approx \sigma_3$) (Simón, 1989; Arlegui et al., 2005; Liesa et al., 2019). Then, we perform and examine analogue models in order to analyse the factors that control fracture development in contexts comparable to such relay zones.

Although laboratory experiments carried out since the 90's have tried to delve into factors that control the development of extensional fault relay zones, they have been systematically performed under uniaxial extension conditions (e.g., Clifton et al., 2000; Mansfield and Cartwright, 2001; Le Calvez and Vendeville, 2002; Acocella et al., 2005; Hus et al., 2005; Athmer et al., 2010). The present paper is -as far as we know-the first one that describes experiments that simulate a biaxial or radial extensional regime.

In addition to the type of stress field in which relay zones develop, spatial stress heterogeneity should also be taken into account. Numerical models (e.g., Simón et al., 1988; Kattenhorn et al., 2000) show that, where previous oblique faults do exist, trajectories of the minimum stress axis (σ_3) undergo sharp deflection, veering to become either parallel to the fault (close to the tips) or perpendicular to it (close to the centre). Swapping of σ_2 and σ_3 axes is also a common phenomenon, which result in e.g. orthogonal joint sets (Simón, 1989). Such a dynamic setting makes the results of analogue modelling less predictable and more exciting, open to a wide range of potential deformation patterns.

2 Geological setting

The eastern Iberian Chain (Fig. 2A) shows a large network of Neogene-Quaternary extensional basins that postdate and obliquely cut its compressive structures (Fig. 2B; Álvaro et al., 1979). They represent the onshore deformation linked to rifting of the Valencia Trough, which is accommodated by a listric extensional fault system detached at a depth of 11–14 km (Roca and Guimerá, 1992)[1]. Such basins evolved through two main extensional episodes (Simón, 1982, 1983): the first episode, Upper Miocene in age, produced NNE-SSW trending grabens (Teruel and Maestrazgo Grabens, parallel to the Valencia Trough); the second one, Upper Pliocene-Present, gave rise to reactivation of the former basins and created the NNW-SSE trending Jiloca Graben.

The Teruel Basin is a half graben controlled by large N–S striking faults located at the eastern boundary (El Pobo and Javalambre mountain fronts; Fig. 2B and C). It is filled with alternating red clastic materials and carbonates, in which several informal lithological units (Rojo 1, Rojo 2 and Rojo 3, clastic; Páramo 1 and Páramo 2, carbonated) have been used by Godoy et al. (1983a,b), Hernández et al. (1983a,b) and Olivé et al. (1983) for mapping purposes (Fig. 2D). This succession culminates with a thin alluvial cover (Villafranchian pediment) that extends over most of the Neogene basins. Their age, well constrained from numerous mammal fossil localities and magnetostratigraphy, ranges from the beginning of the Upper Miocene (Vallesian, 11.2 Ma) up to Upper Pliocene - earliest Pleistocene (Villafranchian, 1.8 Ma; Ezquerro, 2017).

The Jiloca asymmetric graben shows an overall NNW-SSE trend that results from an en-échelon right-releasing arrangement of NW-SE-striking normal faults, the largest ones being located at the eastern boundary: Calamocha, Sierra Palomera and Concud faults (Fig. 2C). A number of Palaeogene folds are obliquely cut by the graben; nevertheless, they are nearly parallel to the Sierra Palomera and Concud faults, which represent the negative inversion of contractive faults associated to those folds, as explained in Sections 3.2 and 3.3. The basin infill is essentially made of an Upper Pliocene-Pleistocene alluvial sequence (with episodic palustrine deposits), underlain at the central sector by an older lutite-carbonate unit attributed to the Upper Miocene-Lower Pliocene (Rubio and Simón, 2007) (Fig. 2D).

The Teruel and Jiloca grabens developed under a tectonic stress field that evolved from (i) uniaxial extension with WNW-ESE trending σ_3 trajectories, prevailing during the first extensional episode (Miocene-Lower Pliocene), to (ii) nearly biaxial or radial extension (σ_1 vertical, $\sigma_2 \approx \sigma_3$) with σ_3 trending nearly WSW-ENE (Fig. 2E), prevailing during the second episode (Upper Pliocene-Quaternary; Simón, 1982, 1989; Arlegui et al., 2005; Liesa et al., 2019). The latter has essentially remained up to the present-day (Herraiz et al., 2000). Nevertheless, both WSW-ENE and WNW-ESE σ_3 directions are recorded all along Pliocene and Quaternary times: the overall biaxial extension stress field has the appearance of being partitioned (in the sense of Simón et al., 2008) into two stress systems with S_{Hmax} axis (maximum horizontal stress) nearly parallel to the Jiloca and Teruel grabens, respectively. Moreover, both directions are linked to the main tectonic stress sources active during Neogene times in eastern Spain: intraplate NNW-SSE compression produced by Africa-Iberia convergence, and WNW-ESE extension induced by rifting at the Valencia Trough (Simón, 1989; Herraiz et al., 2000; Capote et al., 2002; Arlegui et al., 2005).

Mountain massifs all over the region are modelled by two main planation surfaces: Intramiocene Erosion Surface (*IES*; Gutiérrez and Peña, 1976; Peña et al., 1984) and Fundamental Erosion Surface (*FES*, Peña et al., 1984). Within the Teruel Basin, *IES* and *FES* correlate, respectively, with the basal unconformity of the Neogene infill and the top of the youngest lacustrine-palustrine deposits (Páramo 2 unit), with ages 11.2 Ma and 3.7–3.5 Ma (Ezquerro, 2017). Since Upper Pliocene times, the Neogene infill of the Teruel Basin has been deeply excavated by the Alfambra and Turia rivers, giving rise to four main fluvial terrace levels (Peña, 1981; Godoy et al., 1983b) attributed to the Early, Middle, Late Pleistocene and Holocene, respectively (Sánchez Fabre, 1989; Moissenet, 1993; Arlegui et al., 2005; Gutiérrez et al., 2008; Lafuente et al., 2014; Simón et al., 2016, 2017).

Historic and instrumental seismicity of the region is low to moderate. Epicentres are concentrated along N–S striking faults south of Teruel city, the western margin of the Jiloca Graben and its neighbouring Albarracín Range, with a maximum recorded magnitude of Mb = 4.3 (Instituto Geográfico Nacional, 2019). Most of the available focal mechanisms correspond to normal faults and are consistent with the recent stress field (Herraiz et al., 2000).

3 Master faults

3.1 Calamocha fault

The Calamocha Fault is 17.0 km long, strikes NNW-SSE, dips ca. 70°–75°W, and shows pure normal movement. It sinks the northern sector of the Jiloca Graben with respect to the Neogene infill of the neighbouring Calatayud basin (Fig. 2C). Offset of the Lower Pliocene Páramo 2 unit allows calculating the maximum net slip, which at the central segment (where it splits into four synthetic ruptures) has been calculated to be ca. 220 m (Rubio and Simón, 2007; Martín-Bello et al., 2014). Fault movement initiated in Upper Pliocene times, showing an average slip rate of 0,06-0,09 mm/a.

Two outcrops studied close to Calamocha town evince that the fault has undergone recurrent movement during the Late Pleistocene (prior to 53.1 ka BP, and younger than 69.9 ka, 35.3 ka y 11.1 ka BP (Simón et al., 2012; Martín-Bello et al., 2014).

3.2 Sierra Palomera fault

The Sierra Palomera Fault is a 15.6 km long, NNW-SSE striking normal fault that constitutes the central sector of the Jiloca Graben, associated to the eastern limb of a Paleogene E-verging anticline (Fig. 2C). The fault surface dips between 54° and 87°W; the slickenlines observed on it indicate a nearly pure normal movement with transport direction towards WSW (García-Lacosta et al., 2014).

Unfortunately, it is not possible to gain precise knowledge of the displacement on the Sierra Palomera normal fault as neither Neogene nor Quaternary stratigraphic marker can be recognized in both walls. Nevertheless, the morphotectonic setting clearly reveals significant activity since Upper Pliocene time (mainly manifested by tilting and offset of the Fundamental Erosion Surface), which allows estimating a throw in the range of 350–400 m (Rubio and Simón, 2007; García-Lacosta et al., 2014).

A minor antithetic fault, induced by rollover bending associated to the Sierra Palomera Fault, shows evidence of activity during Late Pleistocene time (García-Lacosta et al., 2014).

3.3 Concud fault

The Concud Fault is 14.2 km long, showing an overall NW–SE strike that veers towards NNW–SSE near its northern and southern tips, where it approaches the Teruel Fault (Fig. 2B). The fault surface tipically dips 65-70° SW. The observed slickenlines indicate (i) a nearly pure normal slip in the central sector, and (ii) an oblique slip in the southern, NNW–SSE striking one (striation pith around 75ºS), both consistent with average bulk transport direction towards N220ºE (Lafuente et al., 2011, 2014).

The Concud Fault follows the vertical to overturned limb of a NW-SE trending, NE-verging anticline, and represents the negative inversion of a previous thrust with an associated propagation anticline (Lafuente et al., 2011, 2014). The extensional fault cross-cuts the previous Upper Miocene-Lower Pliocene infill of the Teruel Basin. The sedimentation was interrupted on its footwall by mid Pliocene time, while a complete syntectonic sequence belonging to the Villafranchian (lacustrine carbonates and red alluvial sediments) and Pleistocene (fluvial terraces and alluvial fans) was deposited on the hanging wall (Simón, 1983; Moissenet, 1985; Ezquerro et al., 2012). The accumulated net displacement since latest Ruscinian time (3.5 Ma; Ezquerro, 2017) is estimated within the range of 255–290 m, resulting in a net slip rate of 0.07–0.08 mm/a (Lafuente et al., 2011, 2014).

Paleoseismological studies indicate that this fault underwent at least eleven events since ca. 74 ka BP, with an average recurrence period of 7.1–8.0 ka. The net accumulated slip during this time lapse has been calculated to 20.5 m, with average coseismic slip of 1.9 m and net slip rate of 0.29 mm/a (Lafuente et al., 2011, 2014; Simón et al., 2016).

3.4 Teruel Fault

The Teruel Fault is a N–S striking, 9.0 km-long, intrabasinal fault that offsets the Neogene infill of the Teruel Basin (Fig. 2B). In detail, it shows a single, N170ºE trending trace at the northern sector, while southwards it branches off into several fault traces whose trends range between NNE-SSW and NNW-SSE. The exposed rupture surfaces dip 68° in average, and striations indicate a nearly pure normal movement with transport direction towards N275ºE (Simón et al., 2017).

The hanging-wall block shows a roll-over structure revealed by tilting (2° E) of the Páramo 2 unit, which involves a minimum throw of ca. 250 m and a net slip of ca. 270 m. This displacement has been partially accommodated by a bending monocline (dipping up to 17º-30° W), which in combination with the roll-over gives rise to a synform sag parallel to the fault (Lafuente et al., 2011). Taking into account an age of ~3.5 Ma (latest Ruscinian) for the Páramo 2 unit at this area (Ezquerro, 2017), it results in a slip rate of ca. 0.075 mm/a.

The Teruel Fault shows a remarkable Pleistocene activity, but its paleoseismic record is quite limited. Four events occurred between 76.0 and 9.2 ka BP have been recorded from trenching in two distinct fault branches, involving a limited slip rate of ca. 0.04 mm/a (Simón et al., 2017).

4 Methodology

4.1 Structural methods

Minor faults and fractures developed within the three large relay zones at the eastern border of the Jiloca Graben have been mapped with the help of aerial photographs and orthoimages, obtaining geological maps at scales around 1:160.000 and 1:40.000. Published maps (by the Spanish geological survey, IGME) at 1:50000 scale (Martín et al., 1977, 1979; Godoy et al., 1983a, 1983b; Hernández et al., 1983a, 1983b; Olivé et al., 1983 ; Ramírez et al., 1983) have been used as a start point. Field survey has also been carried out within specific sectors, in order to improve certain map details, to elaborate cross-sections and to characterize deformation structures. To infer the kinematics of these structures at an outcrop scale, data of minor faults and fractures (rupture planes and slickenlines) have been collected when possible, as well as evidence of displacement of stratigraphic markers or the arrangement of reoriented pebbles, among others.

Rose diagrams of faults and fractures have been elaborated using Stereonet software (Allmendinger et al., 2013; Cardozo and Allmendinger, 2013). Rupture orientations have been measured at two different scales: (i) fractures and minor faults at outcrop scale in a total of 22 data sites, all of them located within Neogene and Quaternary materials; (ii) faults at map scale, either those located within relay zones or the master faults themselves, measured considering their orientation changes along their total lengths.

Many of these ruptures are nearly vertical and do not show any evidence of slip. They have been interpreted as tension (Mode 1) fractures, so extension trajectories have been inferred orthogonal to them. In the case of dipping rupture planes, the insufficient number of slickenlines has made impractical the application of classical methods of paleostress inversion based on fault population analysis. Nevertheless, this type of studies has been extensively carried out in the Jiloca Graben and the surrounding region (e.g., Simón, 1989; Arlegui et al., 2005 ; Liesa et al., 2019). Therefore, our knowledge of the recent regional stress field provides a comprehensive dynamical framework for the investigated fault relay zones.

4.2 Analogue modelling

The analogue models presented in this work are performed in normal gravitational field and are representative of the upper crust, or part of it, in an area subject to biaxial extension. The experimental set-up used for simulating fault relay evolution consists of a basal latex sheet that is fixed by two of its orthogonal ends and, in the other two ends, attached to two mobile walls pushed at constant velocity by stepper motors (Fig. 3A). Models lie centred over the latex sheet and consist of a 0.5-cm-thick silicone strip (~ 25 × 10.8 cm in plan view) overlain by a 1-cm-thick sand pack (25 × 25 cm square in plan view). By moving the two mobile walls away from the two fixed ones, the latex sheet was stretched producing extension in two orthogonal directions of the overlying model. The stepped-shape of the silicone strip in plan view (Fig. 3B) allows generating four main structures and two relay zones in each model, following the configuration proposed by Hus et al. (2005). For this purpose, the function of the silicone strip boundaries is to control nucleation of the main structures. The novelty of our models lies in the application of a biaxial extension regime to study the fracturing evolution of fault relay zones, and to study the influence of two parameters in their development: 1) the regional biaxial extensional regime, and 2) the orientation of the main structures (generated over the silicone strip boundaries).

To represent the brittle behaviour, we used dry sand (Silica Sand L-70/80 S from Sibelco Hispania), with a 99% of SiO_2, grain size between 63 and 400 μm, mean density of 1610 kg m^{-3}, and an internal friction angle of 30º-37° (Román-Berdiel et al., 2019). Sand is a proper material, as it behaves according to the Mohr-Coulomb criterion and shows low cohesion and internal friction angle similar to natural rocks (Mandl et al., 1977; Krantz, 1991; Schellart, 2000; Panien et al., 2006; Klinkmüller et al., 2016). To represent the ductile behaviour, we used colourless silicone putty (Rhodorsil Gomme FB type from Caldic), which is almost perfectly Newtonian at the strain rates imposed in the experiments, that has a viscosity of 7 × 10^3 Pa s at 20 °C and a density of 980 kg m^{-3} (Table 1). It allows simulating the plasticity of a possible detachment level of claystones and evaporites (Weijermars y Schmeling, 1986; RudolfBoutelier et al., 2016).[2]

alt-text: Table 1

Table 1

The presentation of Tables and the formatting of text in the online proof do not match the final output, though the data is the same. To preview the actual presentation, view the Proof.

Scaling parameters between analogue models and nature.

Parameter	Model value	Nature value	Model/nature ratio
Length (L)	0.01 m	800 m	1.25×10^{-5}
Density (ρ)	980–1610 kg/m^3	2000–2700 kg/m^3	$\sim$ 0.5
Gravity (g)	9.8 m/s^2	9.8 m/s^2	1
Stress ($\sigma = \rho gL$)	96–158 Pa	16×10^6 – 21×10^6 Pa	6.25×10^{-6}
Viscosity (μ)	7×10^3 Pa s	1×10^{19} Pa s (Koyi, 1988)	7×10^{-16}
Strain rate ($\varepsilon = \sigma/\mu$)	1.37×10^{-2}–2.22×10^{-2} s	1.6×10^{-12}-2.1×10^{-12} s	8.93×10^9
Internal friction angle	30° - 37°	31° - 40° (Bahroudi et al., 2003)	$\sim$ 1
Velocity ($V = \varepsilon L$)	1.36×10^{-5} – 3.25×10^{-5} m s^{-1}	1.22×10^{-10} - 2.93×10^{-10} m s^{-1}	1.11×10^5
Time ($t = 1/\varepsilon$)	3600 s	3.15×10^{13} s	1.14×10^{-10}

A grid of squared passive sand markers drawn over the sand packs allowed analysing superficial deformation during experiments. This grid is drawn parallel to the directions in which the traction is exerted and, therefore, to the primary extension trajectories. Progressive evolution of the surficial structures has been studied thanks to photographs taken at regular time intervals while running experiments.

Models are geometrically, kinematically and dynamically scaled following principles discussed by Hubbert (1937) and Ramberg (1981). We chose a length ratio of 1.25×10^{-5}, so that 1 cm in the models is equivalent to 0.8 km in nature. Gravity field, densities and viscosities are imposed in the models by the experimental conditions and materials used (Table 1). The models are performed in normal gravitational field (g = 1), and the ratio of densities between model and natural materials is $\rho \sim 0.5$. Proportionality between tectonic and gravitational forces is $\sigma = \rho\ g\ L \sim 6.25 \times 10^{-6}$ and the scale factor for the viscosity of the ductile level $\mu = 7 \times 10^{-16}$. The temporal relationship is $T = 1.14 \times 10^{-10}$ (1 h of experiment represents 1 Ma in nature), and the ratio of velocity is $V = 1.11 \times 10^5$ (the velocity ranges used in the laboratory, between 4.9 and 11.7 cm/h, represent velocity ranges between 0.38 and 0.92 cm/year in nature).

A total of eight experiments have been carried out, which are divided into two series of three models each (Series 1 and Series 2, Table 2) following a preliminary set of two reference models (R1 and R2, Table 2). The main difference between Series 1 and 2 is the ratio of velocities of both motors: 11.7/4.9 and 10.1/8.0, respectively (Table 2). In this way, Series 2 involves a lower horizontal differential stress ('more biaxial') than Series 1. The three models that make up each series differ in the orientation of the silicone strip to the stretching directions.

alt-text: Table 2

Table 2

The presentation of Tables and the formatting of text in the online proof do not match the final output, though

the data is the same. To preview the actual presentation, view the Proof.

Model characteristics and experimental conditions for the different experiments performed. SST = silicone strip thickness; SPT = sand pack thickness; OSS = orientation of the silicone strip; VM1 = velocity of Motor 1; VM2 = velocity of Motor 2; EM1 = total displacement of Motor 1; EM2 = total displacement of Mot[Instruction: On the PDF version, right columns of Table 2 are too spaced to the Series 1 and Series 2 left column. Right columns could be more homogeneously spaced, and closer to the left column.
]or 2.

Experiments		SST (cm)	SPT (cm)	OSS (to M1 extension)	VM1 (cm/h)	VM2 (cm/h)	VM1/VM2 (%)	EM1 (cm)	EM2 (cm)
Series 1	R-1	–	–	–	11.7	4.9	~ 40	20	9
	B1-1	0.5	1	90°	11.7	4.9	~ 40	20	9
	B1-2	0.5	1	115°	11.7	4.9	~ 40	20	9
	B1-3	0.5	1	65°	11.7	4.9	~ 40	20	9
Series 2	R-2	–	–	–	10.1	8	~ 80	14	12.5
	B2-1	0.5	1	90°	10.1	8	~ 80	14	12.5
	B2-2	0.5	1	115°	10.1	8	~ 80	14	12.5
	B2-3	0.5	1	65°	10.1	8	~ 80	14	12.5

In reference models R1 and R2 it was possible to study the deformation fields applied to the latex sheet, which are then transmitted to sand packs of models from Series 1 and 2, respectively. They allowed enclosing a central domain with virtually homogeneous extension where models can be preferably analysed, avoiding possible extension perturbations induced near the fixed boundaries of the latex sheet. These reference models aimed to define the actual deformation field within the latex sheet from a number of circumferences traced on it and then distorted into deformation ellipses under the imposed extension (Fig. 4). Their maximum axes defined extension trajectories that are key elements for subsequent interpretation of structures developed in the sand packs. For detailed analysis of the developed structures, the total length of each single structure has been divided into segments of different orientation. The orientation of each segment is then compared with both the normal to the extension trajectories at that point (γ angle), and the orientation of the silicone strip (θ angle) (Fig. 5). Each individual segment is considered to be controlled by the extensional field when γ is less than $\pm 20°$, and controlled by the orientation of the silicone strip (therefore by the orientation of the main structures) when θ is less than $\pm 20°$.

5 Fracture patterns within fault relay zones

5.1 Northern relay zone: Between Calamocha and Sierra Palomera faults

The northern sector of the relay zone between Calamocha and Sierra Palomera faults shows ruptures that mainly affect the Neogene series, as these units dominate within this sector and belong to the Calatayud Basin infill (Fig. 6). On the contrary, its southern sector shows Mesozoic and Palaeogene units affected by folds that trend parallel to the master faults. The whole relay zone exhibits a mixed style, combining features of *soft linkage* (a gentle relay ramp) and incipient *hard linkage* (through short transverse faults) in some sectors.

Jurassic materials in the central part of the relay zone are cut by nearly N–S striking faults that bound narrow grabens infilled with Quaternary sediments (Capote et al., 1981; Gutiérrez et al., 1983). A well-exposed fault within this graben system, the Rubielos de la Cérida Fault (Site 9; Fig. 6), has been studied in an exceptional outcrop where the rupture surface shows average orientation N 175° E and slickenlines indicating a mean transport direction of the hanging-wall block towards WNW (Site 9; Fig. 6; Capote et al., 1981). Northwest of that horst-and-graben system, nearly N–S striking fractures (Site 7A; Fig. 6) and faults (Site 7B; Fig. 6) also cut Neogene materials.

Neogene conglomerates at the northern part of this relay zone are affected by a main set of faults and fractures oriented around NE-SW (nearly parallel to the map-scale Bañón Fault), accompanied by a second near-orthogonal set oriented NW-SE (Sites 1, 2, 4, 5 and 6; Fig. 6).

Several Quaternary alluvial fans sourced at the map-scale faults spread out towards the centre of the Jiloca Graben. One of them is cut by scattered fractures with a dominant NW-SE to NNW-SSE direction (Site 8; Fig. 6).

5.2 Central relay zone: Between Sierra Palomera and Concud faults

The geometrical characteristics of this relay zone are similar to those of the former one, with a relay ramp similar in size and several fractured sectors in between. Neogene materials predominate within this relay zone, affected by fractures that have been measured in ten outcrops (Fig. 7). Upper Miocene conglomerates are cut by both primary N–S fractures and secondary E-W fractures that locally abut the former ones (Site 2; Fig. 7). Sets of faults and fractures oriented close to N–S offset Mio-Pliocene limestones at Sites 6, 7, 8, 9, and, with a notable density, in Site 10 (see photograph in Fig. 7). The Upper Pliocene sequence is affected by NNW-SSE to N–S striking fractures at Sites 1A and 3 (Fig. 7), and unconformably overlain by the Villafranchian pediment that is cut by NNW-SSE ones (Site 1B; Fig. 7; Simón, 1983). Two small areas for which Ezquerro (2017) provides detailed mapping of Neogene fractures (Sites 4, 5; Fig. 7) show distinct patterns: while N–S striking fractures strongly dominate the middle Miocene of the central sector of the relay zone (Site 4), NW-SE ones prevail at the propagation of Sierra Palomera fault zone, cutting Lower Miocene materials (Site 5).

Larger-scale faults in the northern part of the relay zone mainly affect Paleogene materials, but show Quaternary fans associated to their fault scarps. They are aligned with the possible southern propagation of one branch of the Sierra Palomera Fault, mantaining its NW-SE orientation.

5.3 Southern relay zone: Between Concud and Teruel faults

This relay zone is much smaller than the previous ones; the distance between both fault tips is less than 1 km. The displacement is sharply transferred between both faults through a northwards dipping relay ramp, as shown in their displacement-length profiles (Lafuente et al., 2011). Upper Pliocene and Pleistocene materials are affected by faults and fractures oriented NNW-SSE and occasionaly NNE-SSW, which have been studied in three representative outcrops (Fig. 8). Two additional NNW-SSE striking faults, aligned with a hypothetic northern propagation of the Teruel Fault, have also been detected in the northern sector by means of a geophysical survey (magnetometry and georadar, GPR; Peiro et al., 2017).

Data site 1 includes a main fault zone (1B; Fig. 8), striking NNE-SSW and showing a total throw of 18 m, accompanied by NNW-SSE minor faults and NNE-SSW to N–S fracture sets at its footwall and hanging-wall blocks, respectively (1A,C; Fig. 8). The main ruptures are antithetic to the Concud and Teruel faults and show transport directions of the hanging-wall block towards ENE (Peiro et al., 2017).

Three conspicuous faults showing decametre-scale throw crop out at Las Ramblillas area (Fig. 8), two of them synthetic and one antithetic to the Concud and Teruel faults. The western synthetic fault has an average orientation 157, 48 W and striations that pitch 70 S (Simón et al., 2017).

Fractures at Site 2 (Fig. 8) affect both a Middle Pleistocene and a Late Pleistocene fluvial terrace. The former is offset by a fault that shows a minimum throw of 7 m and a roll-over monocline at its hanging-wall block. The latter shows several normal faults and fractures arranged in a conjugate pattern, all of them striking around NW-SE (Peiro et al., 2019).

6 Experimental results

Several analogue models (Series 1 and Series 2), as well as the preliminary reference models (R1 and R2), have been performed and analysed. Velocities of both motors are distinct in Series 1 and similar to each other in Series 2 (Table 2), so that the velocity setting in Series 2 is supposed to simulate more accurately the nearly biaxial or radial extensional stress field at the eastern Iberian Chain.

Boundary fault systems, as well as deformation structures within relay zones, have successfully developed in all the experiments. They consist in either a single fault system, a graben system, or a combination of both (from now these structures will be named as “master faults”; Fig. 9). Models of Series 1 are characterised by pervasive deformation developed not only within the boundary fault systems but also over the central sector of the silicone strip, where a graben system has been generated (models B1-1, B1-2 and B1-3; Fig. 9). In contrast, in Series 2 deformation is concentrated within the boundary fault zones, and therefore within relay zones (models B2-1, B2-2 and B2-3; Fig. 9).

In both series, when the silicone strip is arranged either at 90° (models B1-1 and B2-1; Table 2, Fig. 9) or 115° (models B1-2 and B2-2; Table 2, Fig. 9) to the main extension direction (i.e. M1 in Fig. 9), master faults completely develop along the silicone boundaries. On the contrary, when the silicone strip is arranged at 65° (models B1-3 and B2-3; Table 2, Fig. 9), master faults only develop in half the length of the silicone boundaries.

These results have also been analysed in terms of the main extension trajectories applied in each series (see Fig. 3). On the one hand, when the silicone strip is nearly perpendicular (models B1-1, B1-2) or making a high angle (models B2-1, B2-2) to the main stretching direction (i.e, the silicone boundaries are favorably oriented with respect to the extension trajectories), master faults develop entirely. On the other hand, when the silicone strip makes a low angle to the extension trajectories (models B1-3, B2-3), almost no silicone boundary is favorably oriented and the master faults are hardly developed. These results emphasize the role of the stress/strain trajectories in the resulting fracture pattern, while neglecting the influence of preexisting structures when the latter are not favorably orientated. Such tendency can be recognized even in the case of a nearly biaxial or radial or extensional regime, where a wide range of fracture orientations would be theoretically able to be activated.

Both in Series 1 and 2, interaction between master faults through relay zones occurs from early stages. Fault traces are usually visible between minutes 30 and 50 of the experiments. In some cases, like model B2-2, the faults start growing at the segments that define the relay zone and then spread to more distant points (Fig. 10A and B). This allows accommodating deformation in a greater extent near the relay zones and, as a result, relay ramps develop (Figs. 9, 10C and 11A; Walsh and Watterson, 1991). At intermediate stages, some relay zones evolve through continuous along-strike propagation of one of the master faults, in several cases with a curved geometry (Figs. 10C and 11B), while bending at the relay ramp increases. At advanced stages, propagation of the master faults continues (Fig. 9 models B1-1, B1-2, B2-2, Fig. 10D) and, especially in models of Series 2 transition to *hard linkage* by means of transverse connecting faults initiate (Figs. 9, 10D and 11C).

alt-text: Fig. 10

Fig. 10

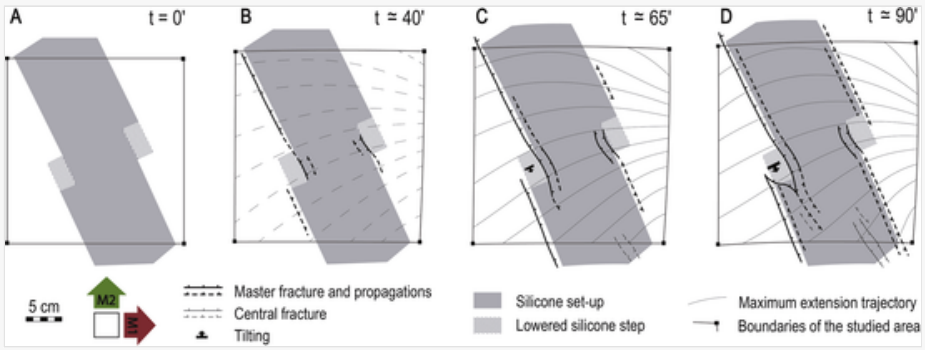

Line drawing of the surface of model B2-2 showing the evolution of deformation.

alt-text: Fig. 11

Fig. 11

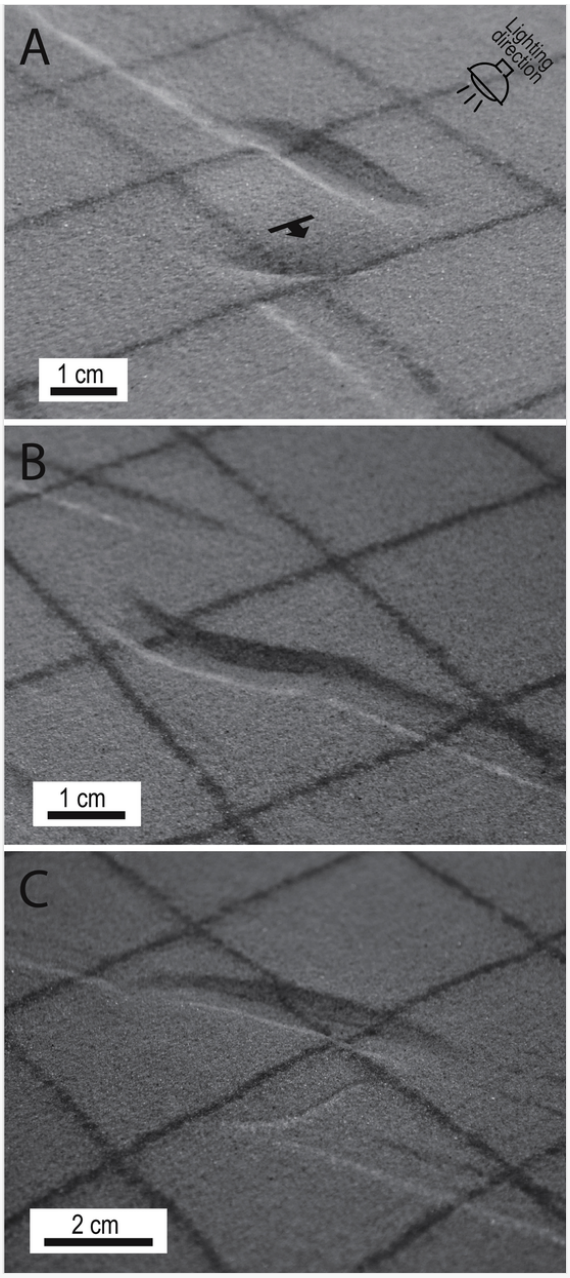

Photographs of the surface of representative models showing deformation in relay ramps. (A) Relay ramp and incipient transverse connecting fault in model B2-1. (B) Curved propagation of one of the main structures in model B1-2. (C) Transverse connecting fault in model B2-2. Lighting direction is [Instruction: Fig. 11 in the PDF version of the manuscript could be made considerably smaller. Reducing the size of this figure, as well as Fig. 5, would contribute to counterbalance the enlargement of others.]indicated.

alt-text: Fig. 12

Fig. 12

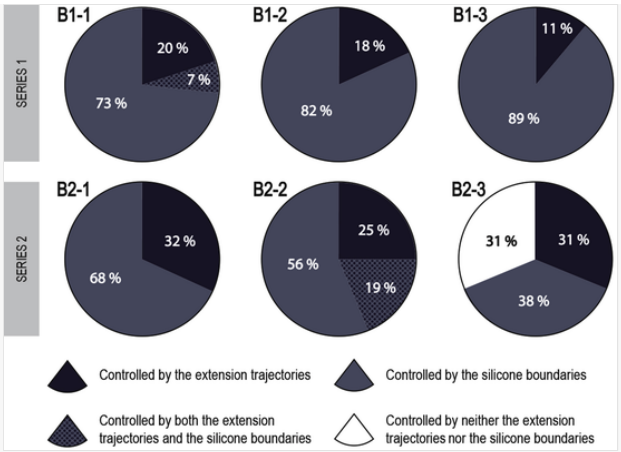

Percentages of accumulated length of boundary fractures developed in the six analogue models performed, depending on whether their orientations are controlled by the extension trajectories or the silicone boundaries.

Nevertheless, it should be noticed that such transverse ruptures are not orthogonal to the master faults, neither oblique in the sense in which they ordinarily arise in models reported in the literature: they make angles >90° with the along-strike propagation of the neighbouring master fault (see Figs. 9, 10D and 11C), which constitutes a remarkable anomaly. When compared with the deformation field recorded in the basal latex sheet, it is observed that those connecting faults are almost orthogonal to the extension trajectories. An actual case of such geometry has been described by Nixon et al. (2019), implicitly assuming that the distributed fractures within the relay zone are directly controlled by the remote stress field.

The compatibility analysis of the resulting structures is shown in Fig. 12, where each pie chart represents the total percentage of accumulated length of boundary fault system developed in each experiment, central fractures are not taken into account in this analysis. The percentages of fracture segments controlled by the silicone strip orientation ($\theta < \pm 20°$) correspond, almost in its entirety, to the main structures directly developed over the boundaries. The percentages controlled by the extension trajectories ($\gamma < \pm 20°$) represent fracture sets developed in relay zones. Thus, both curved propagation of the master faults and fault linkage have been mainly controlled by the extension field.

7 Interpretation and discussion

7.1 Discriminating the influence of external and internal controls over fracture patterns in relay zones

Fracture patterns developed in fault relay zones at the eastern margin of the Jiloca Graben are summarized in rose diagrams of Fig. 13, where strike distributions of (i) fractures and minor faults at outcrop scale, (ii) faults at map scale, and (iii) master faults themselves, have been gathered for each relay zone. In addition, Fig. 14 depicts the interpretation of these rose diagrams in terms of compatibility or incompatibility of the different fracture sets with macrostructure heritage and stress trajectories. Since the general trend of the Jiloca Graben is nearly parallel to S_{Hmax} (Simón, 1989), and its bounding master faults only make a very-low-angle with it, in practice it is not easy to discriminate between ‘ruptures controlled by the primary stress field’ and ‘ruptures

controlled by the structural heritage'. Hence a significant percentage of structures are considered as 'controlled by both of them'. All the same, ruptures of any of these origins, overall oriented in the range of 130–200, can be classified as longitudinal or along-strike fractures and grouped into a single genetic category: 'externally controlled' fractures (types I and J in Fig. 1). The latter are conceptually different from transverse fractures 'internally controlled' by the own relay kinematics and the subsequent stress/strain perturbations (types A, B, C and D in Fig. 1). Intermediate cases in which both external controls and internal kinematics occur are represented by types E, F, G and H in Fig. 1.

alt-text: Fig. 13

Fig. 13

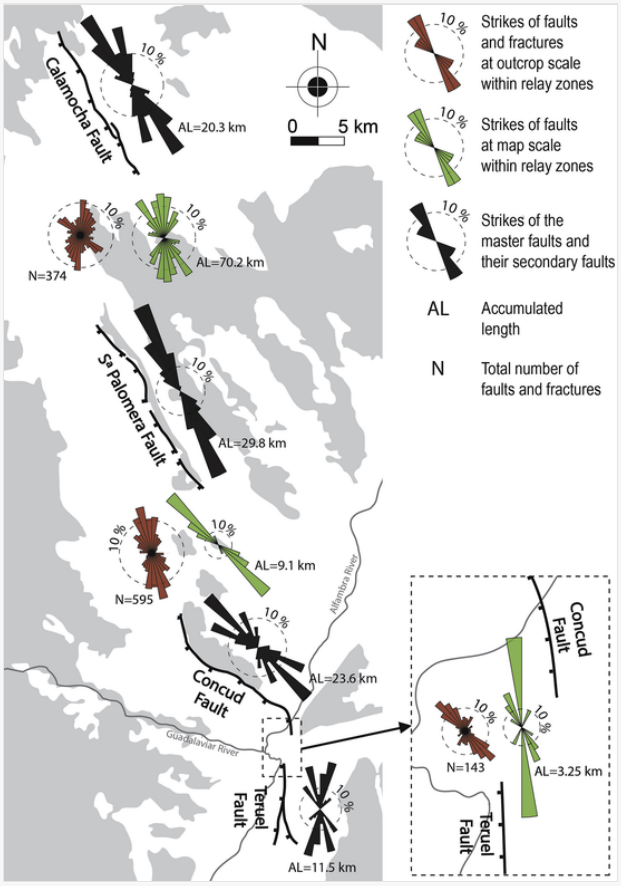

Fault and fracture patterns, at outcrop and map scale, in the relay zones between the Calamocha, Sierra Palomera, Concud and Teruel faults, and the master fault zones [Instruction: On the PDF version, Fig. 13 and 14 are suitably placed together, but their sizes are not the same. If only Fig. 13 was a bit smaller they would appear balanced and aligned.
]themselves.

alt-text: Fig. 14

Fig. 14

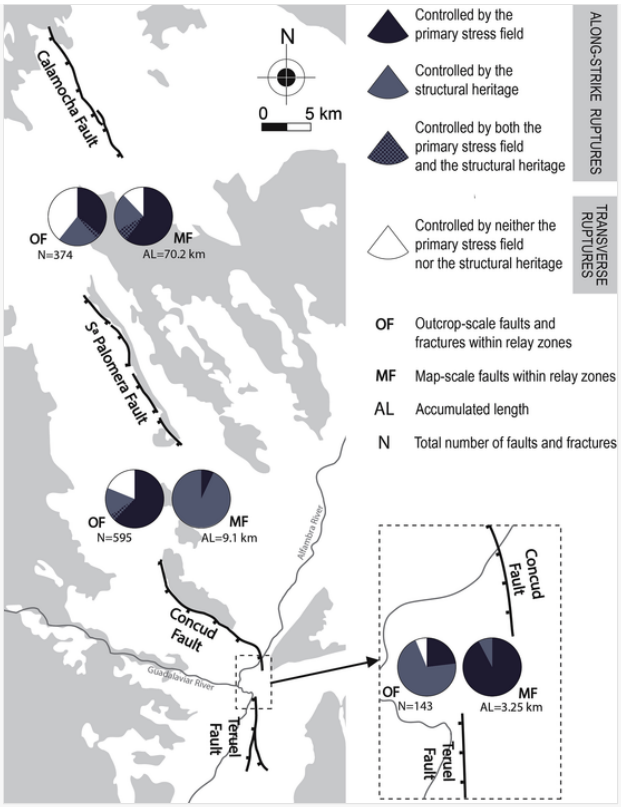

Comparative balance of structural heritage vs. remote stress field as controls of rupture development within the relay zones between the Calamocha, Sierra Palomera, Concud and Teruel faults at outcrop and map scale.

alt-text: Fig. 15

Fig. 15

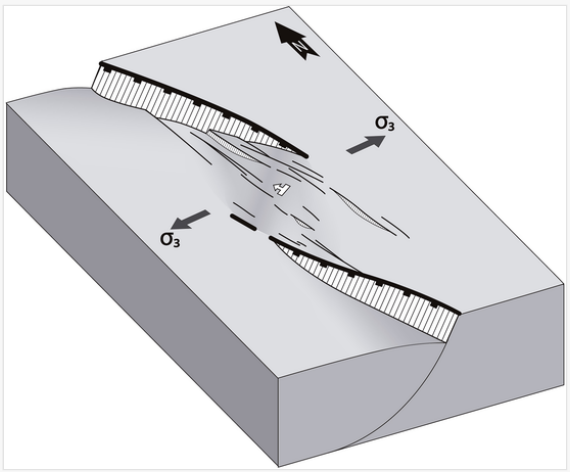

3D conceptual model of relay zone with distributed longitudinal, along-strike propagated fractures, developed under the double influence of the structural heritage and remote stress [Instruction: Fig. 15 should be placed within the 7.2. section, therefore enhancing its role as final visual model presented in this paper.
]field.

Most ruptures within the three studied relay zones are along-strike ones (Figs. 13 and 14). They are quite homogeneously distributed and appear at any scale: (a) in the northern relay zone, 61% and 88% of outcrop and map ruptures, respectively; (b) in the central relay zone, 81% and 100%, and (c) in the southern relay zone, 94% and 100%.

The trend controlled by the primary stress field (Fig. 14) can be recognized among the distributed ruptures at map scale of the northern relay zone (making the large N–S graben system; Fig. 6), that involve Neogene and Quaternary deposits. Within the central relay zone, these fractures are homogeneously distributed at outcrop scale and mainly affect Neogene units (Fig. 7). Within the southern relay zone, map-scale faults are also parallel to both the master faults (Teruel and southern segment of Concud; Fig. 8) and the S_{Hmax} trajectories. The incipient northwards propagation of the Teruel Fault, as inferred from surface data and subsoil geophysical exploration (Fig. 8; Peiro et al., 2017), also follows the same trend. For this reason, a future junction of the Teruel and Concud faults through along-strike propagation of the former till abutting the latter constitutes a reliable prediction (Peiro et al., 2017).

The trend controlled by the structural heritage (Fig. 14) is clearly recognizable in the central relay zone, where map-scale faults follow the NW-SE orientation of the Sierra Palomera Fault (Fig. 7), as well as in the outcrop-scale fractures from the southern relay zone. Although also present in the northern relay zone, such fracture sets represent a minority with respect to the stress-controlled, N–S trending sets.

Significant transverse ruptures have been found only in the northern relay zone (Figs. 6 and 14). The most noticeable structure is the Bañón Fault, which can be considered as an incipient connecting fault. Within the central and southern relay zones, transverse fractures have been observed only at outcrop scale and barely represent 19% and 6% of the total, respectively (Fig. 14).

It could be expected that transverse, even orthogonal, secondary fractures were more common in relay zones within biaxial extension, owing to the frequent swapping of σ_2 and σ_3 axes occurring under such stress regime, as stated in Section 1. Nevertheless, we should remember that such type of stress perturbation, which commonly results in secondary fractures at right angles to the master faults, typically takes place close to central sectors of the latter. In contrast, in the vicinity of the fault tips, σ_3 trajectories tend to either remain or become orthogonal to those master faults (Simón et al., 1988), hence enabling along-strike rupture propagation.

7.2 Fault relay zones evolving through distributed longitudinal fractures: contrasting analogue modelling, nature and literature

The notion of a relay zone evolving through distributed longitudinal fractures, developed under the influence of both inherited faults and the coeval stress regime, and without any significant presence of transverse connecting ruptures, has been corroborated by analogue modelling. When a ‘less biaxial’ extensional field is applied (Series 1), abundant deformation within both the boundary fault zones and the central sectors develops. Under ‘more biaxial’ extension (Series 2), deformation is concentrated close to the master faults and within the relay zones (Fig. 9). But, in general, fracture segments controlled by the ‘structural inheritance’ (silicone strips) or the extension trajectories, i.e. along-strike fractures, clearly dominate in all cases. The

structural evolution of the relay zones corresponds to a *soft linkage* by means of relay ramps from early to intermediate stages, and a *hard linkage* by means of connecting faults at advanced stages (Figs. 10 and 11 A,C). But the latter do not show the angle commonly observed in analogue and numerical models in the literature (≤90° to the along-strike propagation of the master fault). On the contrary, they are nearly orthogonal to the extension trajectories (Figs. 9 and 10D), again revealing the influence of the remote stress/strain field beyond the control of relay kinematics.

The described fracture patterns do not fit those classically reported from numerical and analogue models in the literature. It could be argued that the northern and central relay zones are too wide with respect to the fault length, and that their overlapping distances are null, so that they do not constitute representative cases from which useful conclusions could be obtained. But the same attributes have been observed in the southern relay zone, between the closely spaced Concud and Teruel faults, where the classical transverse connecting faults are absent as well.

Therefore, a new conceptual model of relay zone should be defined (Fig. 15), in which fracture sets mimicking the inherited structural trends or responding to the remote stress field (two factors that have been usually disregarded) prevail over internally induced ones. Some of those along-strike or longitudinal ruptures represent propagation of the master faults, but others develop quite homogeneously all over the relay zone.

The resulting fault pattern exhibits features that have been highlighted in two recent papers by Deng et al. (2017), using numerical models of fault reactivation under oblique extension, and Nixon et al. (2019), on the basis of a detailed study of faults and fractures in Lower Jurassic rocks of the Somerset coast (UK). Nixon et al. (2019) describe how within the relay ramp numerous smaller, nearly parallel and quite homogenously distributed faults and veins ('damage-related fractures') develop under increasing stress perturbations, whereas outside of the relay ramp spatial distribution of deformation is more heterogeneous since it is mostly constrained to the master faults. Such distributed longitudinal ruptures play an important role in fault interaction, accommodating and transferring part of the displacement between the interacting master faults, also maintaining their kinematic coherency. The influence of pre-existing structures adds geometric complexity to the fault network, resulting in an interfering, partially linked ensemble of reactivated faults and ruptures controlled by the remote stress field (Deng et al., 2017).

It is probable that, at relays of active faults, longitudinal ruptures also contribute to modify their seismic behaviour and hence seismic hazard of the region. They can either enable triggering seismic events on the adjacent master fault (hypothetically resulting in alternating slip on both of them, as it has already been suggested for the Concud and Teruel faults; Simón et al., 2017), or move themselves producing minor seisms that release part of the total energy.

Relay ramps with distributed along-strike fractures represent an interaction stage one step beyond bare *soft linkage*. The relay zones between the Calamocha, Sierra Palomera, Concud and Teruel faults are therefore in an intermediate stage between complete independency and coalescence. Such appraisal was already formulated for the Concud and Teruel faults by Lafuente et al. (2011) based on their displacement-length profiles.

Scenarios of future evolution of the studied relay zones can be envisaged in the light of the analogue models. In spite of these being properly scaled, deformation was not visible after applying the amount of extension undergone by the study region. The latter corresponds to a finite elongation of less than a 1% (estimated from total displacements of the Concud, Teruel and Valdecebro faults; Simón et al., 2012) while in analogue models a finite elongation of 12,5% was reached. Since this extension is higher, the advanced stages of analogue models can be interpreted as tentative predictions of evolution of the regional structures. A future *hard linkage* by means of transverse connecting faults is not expected. Instead, fault coalescence will probably occur in the future by propagation of one of the involved faults, giving rise to a final braided fault pattern (Fig. 1J).

8 Conclusions

The Jiloca Graben is an elongated depression in the eastern Iberian Chain, whose eastern margin consists in a right-relay arrangement of three NW-SE normal faults: Calamocha, Sierra Palomera and Concud. They have been active since Pliocene times under a nearly biaxial or radial extension regime, with σ_3 trending nearly WSW-ENE (Arlegui et al., 2005; Ezquerro, 2017). Together with the Teruel Fault, these faults enclose three relay zones that exhibit fracture networks different from those commonly predicted in fault relay models in the literature.

The three relay zones are characterised by transferring part of the displacement through relay ramps, revealing *soft linkage* interaction. But such relay ramps are further cut by distributed faults and fractures at metre to kilometre scales, affecting both Upper Miocene and Quaternary materials, which also contribute to slip transfer and dynamical interaction. Their structural analysis has allowed to identify three main fracture directions: (i) parallel to the master faults that enclose the relay zones (NW-SE to NNW-SSE), (ii) perpendicular to the σ_3 trendings during Neogene and Quaternary times (NNW-SSE to N–S), and (iii) transverse to the macrostructures (NE-SW). Cases (i) and (ii), classified as along-strike ruptures, dominate within the three relay zones. Their relative weight in each zone depends on the influence of the structural heritage and the stress field. Transverse fractures are more scarce and confined to certain sectors.

Analogue modelling has allowed understanding the controls of such fracture patterns. Fractures are mostly controlled by the inherited anisotropies and the coeval extension trajectories, which results in clear prevalence of along-strike fractures in both ‘more biaxial’ and ‘less biaxial’ extension regimes. Although incipient transverse connecting faults occur in advanced stages, they do not show the orientation usually reported in numerical and experimental models, but that controlled (orthogonal to) the remote extension trajectories.

A new conceptual model of fault coalescence through relay zones is defined (Fig. 15), in which externally controlled fracture sets (either parallel to the inherited structural trends, or responding to the remote stress field) prevail over those internally induced by the own relay kinematics.

The Calamocha, Sierra Palomera, Concud and Teruel faults, are interacting and evolving through along-strike fractures distributed within their relay zones, and constitute good examples of such fault relay type. The overall fault system is at an intermediate stage between complete independence and coalescence. Future linkage will probably occur through along-strike (parallel or at very-low-angle) propagation of the master faults, resulting in a braided geometry.

Authors statements

Alba Peiro: Investigation, Methodology, Formal analysis, Writing - Original Draft, Visualization.

José Luis Simón: Conceptualization, Methodology, Investigation, Writing - Review & Editing, Supervision.

Teresa Román-Berdiel: Methodology, Validation, Investigation, Writing - Review & Editing, Supervision.

Declaration of competing interest

The authors declare that they have no known competing financial interests or personal relationships that could have appeared to influence the work reported in this paper.

Acknowledgements

Financial support was granted by the project Geotransfer-E32_17R of the Gobierno de Aragon y[3] Programa Operativo FEDER Aragón 2014–2020.

References

The corrections made in this section will be reviewed and approved by journal production editor.

Acocella, V., Morvillo, P., Funiciello, R., 2005. What controls relay ramps and transfer faults within rift zones? Insights from analogue models. J. Struct. Geol. 27, 397–408.

Allmendinger, R.W., Cardozo, N.C., Fisher, D., 2013. Structural Geology Algorithms: Vectors & Tensors. Cambridge University Press, Cambridge.

Álvaro, M., Capote, R., Vegas, R., 1979. Un modelo de evolución geotectónica para la Cadena Celtibérica. Acta Geol. Hispánica 14, 172–177.

Arlegui, L.E., Simón, J.L., Lisle, R.J., Orife, T., 2005. Late Pliocene-Pleistocene stress field in the Teruel and Jiloca Grabens (eastern Spain): contribution of a new method of stress inversion. J. Struct. Geol. 27, 693–705.

Athmer, W., Groenenberg, R.M., Luthi, S.M., Donselaar, M.E., Sokoutis, D., Willingshofer, E., 2010. Relay ramps as pathways for turbidity currents: a study combining analogue sandbox experiments and numerical flow simulations. Sedimentology 57, 806–823.

Bahroudi, A., Hemin, A.K., Talbot, C.J., 2003. Effect of ductile and frictional dècollements on style of extension. J. Struct. Geol. 25, 1401–1423.

Capote, R., Gutiérrez, M., Hernández, A., Olivé, A., 1981. Movimientos recientes de la fosa del Jiloca (Cordillera Ibérica). V Reunión del Grupo Español de Trabajo del Cuaternario, Sevilla, pp. 245–257.

Capote, R., Muñoz, J.A., Simón, J.L., Liesa, C.L., Arlegui, L.E., 2002. Alpine tectonics I: the alpine system north of the betic cordillera. In: Gibbons, W., Moreno, T. (Eds.), Geology of Spain. The Geological Society, London, pp. 367–400.

Cardozo, N., Allmendinger, R.W., 2013. Spherical projections with OSXStereonet. Comput. Geosci. 51, 193–205.

Cartwrigth, J.A., Trudgill, B.D., Mansfield, C.S., 1995. Fault growth by segment linkage: an explanation for scatter in maximum displacement and trace length data from the Canyonlands Graben of S. E. Utah. J. Struct. Geol. 17, 1319–1326.

Childs, C., Easton, S.J., Vendeville, B.C., Jackson, M.P.A., Lin, S.T., Walsh, J.J., Watterson, J., 1993. Kinematic analysis of faults in a physical model of growth faulting above a viscous salt analogue. Tectonophysics 228, 313–329.

Childs, C., Watterson, J., Walsh, J.J., 1995. Fault overlap zones within developing normal fault systems. J. Geol. Soc. 152, 535–549. London.

Clifton, A.E., Schlische, R.W., Withjack, M.O., Ackermann, R.V., 2000. Influence of rift obliquity on fault-population systematics: results of experimental clay models. J. Struct. Geol. 22, 1491–1509.

Crider, J.G., Pollard, D.D., 1998. Fault linkage: three-dimensional mechanical interaction between echelon normal faults. J. Geophys. Res. 103, 675–692.

Deng, C., Gawthorpe, R.L., Finch, E., Fossen, H., 2017. Influence of a pre-existing basement weakness on normal fault growth during oblique extension: insights from discrete element modeling. J. Struct. Geol. 105, 44–61.

Ezquerro, L., Lafuente, P., Pesquero, M.D., Alcalá, L., Arlegui, L.E., Liesa, C.L., Luque, L., Rodríguez-Pascua, M.A., Simón, J.L., 2012. Una cubeta endorreica residual Plio-pleistocena en la zona de relevo entre las fallas de Concud y Teruel: implicaciones paleogeográficas. Rev. Soc. Geol. Espana 25, 157–175.

Ezquerro, L., 2017. El sector norte de la cuenca neógena de Teruel: tectónica, clima y sedimentación Ph.D. thesis. Universidad de Zaragoza.

Ferrill, D.A., Morris, A.P., 2001. Displacement gradient and deformation in normal fault systems. J. Struct. Geol. 23, 619–638.

Finzi, Y., Langer, S., 2012. Damage in step-overs may enable large cascading earthquakes. Geophys. Res. Lett. 39, L16303. doi:10.1029/2012GL052436.

Fossen, H., Rotevatn, A., 2016. Fault linkage and relay structures in extensional settings - a review. Earth Sci. Rev. 154, 14–28.

Fossen, H., Johansen, T.E.S., Hesthammer, J., Rotevatn, A., 2005. Fault interaction in porous sandstone and implications for reservoir management; examples from Southern Utah. Bull. Am. Assoc. Pet. Geol. 89, 1593–1606.

García-Lacosta, A.I., Pueyo, Ó., Arlegui, L.E., Liesa, C.L., Ezquerro, L., Simón, J.L., 2014. La zona de falla reciente de Sierra Palomera (fosa del Jiloca, Cordillera Ibérica): contribución de la geofísica a la caracterización estructural. In: 2ª Reunión Ibérica sobre Fallas Activas y Paleosismología. pp. 51–54. Lorca.

Gawthorpe, R., Hurst, J.M., 1993. Transfer zones in extensional basins: their structural style and influence on drainage development and stratigraphy. J. Geol. Soc. 150, 1137–1152.

Gawthorpe, R., Leeder, M.R., 2000. Tectono-sedimentary evolution of active extensional basins. Basin Res. 12, 195–218.

Gawthorpe, R.L., Jackson, C.A.L., Young, M.J., Sharp, I.R., Moustafa, A.R., Leppard, C.W., 2003. Normal fault growth, displacement localisation and the evolution of normal fault populations: the Hammam Faraun fault block, Suez rift, Egypt. J. Struct. Geol. 25, 883–895.

Gibbs, A.D., 1984. Structural evolution of extensional basin margins. J. Geol. Soc. 141, 609–620.

Gibbs, A.D., 1990. Linked fault families in basin formation. J. Struct. Geol. 12, 795–803.

Godoy, A., Moissenet, E., Ramírez, J.I., Olivé, A., Aznar, J.M., Jerez, L., Aragonés, E., Aguilar, M.J., Ramírez del Pozo, J., Leal, M.C., Adrover, R., Alberdi, M.T., Giner, J., Gutiérrez, M., Portero, J.M., Gabaldón, V., 1983. Mapa Geológico de España 1: 50.000. Instituto Geológico y Minero, Madrid. Hoja 542 (Alfambra).

Godoy, A., Ramírez, J.I., Olivé, A., Moissenet, E., Aznar, J.M., Aragonés, E., Aguilar, M.J., Ramírez del Pozo, J., Leal, M.C., Jerez Mir, L., Adrover, R., Goy, A., Comas, M.J., Alberdi, M.T., Giner, J., Gutiérrez Elorza, M., Portero, J.M., Gabaldón, V., 1983. Mapa Geológico de España 1: 50.000. Instituto Geológico y Minero, Madrid. Hoja 567 (Teruel).

Gutiérrez, F., Gutiérrez, M., Gracia, F.J., McCalpin, J.P., Lucha, P., Guerrero, J., 2008. Plio-Quaternary extensional seismotectonics and drainage network development in the central sector of the Iberian Chain (NE Spain). Geomorphology 102, 21–42.

Gutiérrez, M., Peña, J.L., 1976. Glacis y terrazas en el curso medio del río Alfambra (provincia de Teruel). Bol. Geol. Min. 87, 561–570.

Gutiérrez, M., Peña, J.L., Simón, J.L., 1983. Los valles tectónicos recientes de Rubielos de la Cérida (Teruel). Cuad. do Lab. Xeoloxico Laxe 5, 449–459.

Gupta, A., Scholz, C.H., 2000. A model of normal fault interaction based on observations and theory. J. Struct. Geol. 22, 865–879.

Hernández, A., Olivé, A., Moissenet, E., Pardo, G., Villena, J., Portero, J.M., Gutiérrez, M., Puigdefábregas, C., Giner, J., Aguilar, M.J., Leal, M.C., Gutiérrez, J.C., Gil, M.D., Adrover, R., Gabaldón, V., 1983. Mapa Geológico de España 1: 50.000. Instituto Geológico y Minero, Madrid. hoja 491 (Calamocha).

Hernández, A., Ramírez, J.I., Olivé, A., Riba, O., Aragonés, E., Aguilar, M.J., Ramírez del Pozo, J., Leal, M.C., Giner, J., Gutiérrez, M., Goy, A., Comas, M.J., Gutiérrez, J.L., Portero, J.M., Gabaldón, V., 1983. Mapa Geológico de España 1: 50.000. Instituto Geológico y Minero, Madrid. hoja 566 (Cella).

Herraiz, M., De Vicente, G., Lindo-Ñaupari, R., Giner, J., Simón, J.L., González-Casado, J.M., Vadillo, O., Rodríguez-Pascua, M.A., Cicuéndez, J.L., Casas, A., Cabañas, L., Rincón, P., Cortés, A.L., Ramírez, M., Lucini, M., 2000. The recent (upper Miocene to Quaternary) and present tectonic stress distributions in the Iberian Peninsula. Tectonics 19, 762–786.

Hubbert, M.K., 1937. Theory of scale models as applied to the study of geologic structures. Bull. Geol. Soc. Am. 48, 1459–1519.

Huggins, P., Watterson, J., Walsh, J.J., Childs, C., 1995. Relay zone geometry and displacement transfer between normal faults recorded in coal-mine plans. J. Struct. Geol. 17, 1741–1755.

Hus, R., Acocella, V., Funiciello, R., De Batist, M., 2005. Sandbox models of relay ramp structure and evolution. J. Struct. Geol. 27, 459–473.

Instituto Geográfico Nacional. Servicio de Información Sísmica del Instituto Geográfico Nacional. https://www.ign.es/web/ign/portal/sis-catalogo-terremotos, 2019.

Kattenhorn, S.A., Aydin, A., Pollard, D.D., 2000. Joints at high angles to normal fault strike: an explanation using 3-D numerical models of fault-perturbed stress fields. J. Struct. Geol. 22, 1–23.

Klinkmüller, M., Schreurs, G., Rosenau, M., Kemnitz, H., 2016. Properties of granular analogue materials: a community wide survey. Tectonophysics 684, 23–38.

Koyi, H., 1988. Experimental modelling of role of gravity and lateral shortening in Zagros mountain Belt. Am. Assoc. Petrol. Geol. Bull. 72, 1381–1394.

Krantz, R.W., 1991. Measurements of friction coefficients and cohesion for faulting and fault reactivation in laboratory models using sand and sand mixtures. Tectonophysics 188, 203–207.

Lafuente, P., Arlegui, L.E., Casado, I., Ezquerro, L., Liesa, C.L., Pueyo, O., Simón, J.L., 2011. Geometría y cinemática de la zona de relevo entre las fallas neógeno-cuaternarias de Concud y Teruel (Cordillera Ibérica). Rev. la Soc. Geol. España 24, 109–125.

Lafuente, P., Arlegui, L.E., Liesa, C.L., Pueyo, O., Simon, J.L., 2014. Spatial and temporal variation of paleoseismic activity at an intraplate, historically quiescent structure: the Concud Fault (Iberian Chain, Spain). Tectonophysics 632, 167–187.

Le Calvez, J.H., Vendeville, B.C., 2002. Experimental designs to model along-strike fault interaction. J. Virtual Explor. 7, 1–17.

Liesa, C.L., Simón, J.L., Ezquerro, L., Arlegui, L.E., Luzón, A., 2019. Stress evolution and structural inheritance controlling an intracontinental extensional basin: the central-northern sector of the Neogene Teruel Basin. J. Struct. Geol. 118, 362–376.

Machette, M.N., Personius, S.F., Nelson, A.R., 1991. The Wasatch fault zone Utah: segmentation and history of Holocene earthquakes. J. Struct. Geol. 13, 137–150.

Mandl, G., De-Jong, L.N.J., Maltha, A., 1977. Shear zones in granular material; an experimental study of their structure and mechanical genesis. Rock Mech. 9, 95–144.

Manighetti, I., Zigone, D., Campillo, M., Cotton, F., 2009. Self-similarity of the largest-scale segmentation of the faults: implications for earthquake behavior. Earth Planet. Sci. Lett. 288, 370–381.

Mansfield, C., Cartwright, J., 2001. Fault growth by linkage: observations and implications from analogue models. J. Struct. Geol. 23, 745–763.

Martín, M., Canerot, J., Del Pan, T., Leyva, F., 1979. Mapa Geológico de España 1:50.000. Instituto Geológico y Minero, Madrid. hoja 517 (Argente).

Martín, M., Canerot, J., Linares-Rivas, A., Grambast, L., Quintero, I., Mansilla, H., De las Heras, A., Fernández, M.C., Leyva, F., Martínez, J.U., 1977. Mapa Geológico de España 1: 50.000. Instituto Geológico y Minero, Madrid. hoja 492 (Segura de los Baños).

Martín-Bello, L., Arlegui, L.E., Ezquerro, L., Liesa, C.L., Simón, J.L., 2014. La falla de Calamocha (fosa del Jiloca, Cordillera Ibérica): estructura y actividad pleistocena. In: 2ª Reunión Ibérica sobre Fallas Activas y Paleosismología. pp. 55–58. Lorca.

Moissenet, E., 1985. Les dépressions tarditectoniques des Chaînes Ibériques méridionales: distension, diapirisme et dépôts associés. Compte Rendus de l'Academie du Sciences de Paris 11, 523–528.

Moissenet, E., 1993. L'age et les déformations des terrases alluviales du Fossé de Teruel. In: El. Cuaternario de España y Portugal, I. Instituto Geológico y Minero de España-AEQUA, Madrid, pp. 267–279.

Morley, C.K., Wonganan, N., 2000. Normal fault displacement characteristics, with particular reference to synthetic transfer zones, Mae Moh mine, northern Thailand. Basin Res. 12, 307–327.

Moustafa, A.R., Khalil, S.M., 2016. Control of extensional transfer zones on syntectonic and post-tectonic sedimentation: implications for hydrocarbon exploration. J. Geol. Soc. 174 (2), 318–335.

Nicol, A., Walsh, J., Berryman, K., Nodder, S., 2005. Growth of a normal fault by the accumulation of slip over millions of years. J. Struct. Geol. 27, 327–342.

Nixon, C.W., Vaagan, S., Sanderson, D.J., Gawthorpe, R.L., 2019. Spatial distribution of damage and strain within a normal fault relay at Kilve, UK. J. Struct. Geol. 118, 194–209.

Olivé, A., Hernández, A., Moissenet, E., Pardo, G., Villena, J., Gutiérrez, M., Puigdefábregas, C., Giner, J., Aguilar, M.J., Leal, M.C., Goy, A., Comas, M.J., Adrover, R., Portero, J.M., Gabaldón, V., 1983. Mapa Geológico de España 1: 50.000. Instituto Geológico y Minero, Madrid. hoja 516 (Monreal del Campo).

Panien, M., Schreurs, G., Pfiffner, A., 2006. Mechanical behaviour of granular materials used in analogue modelling: insights from grain characterization, ring-shear tests and analogue experiments. J. Struct. Geol. 28, 1710–1724.

Peacock, D.C.P., 2002. Propagation, interaction and linkage in normal fault systems. Earth Sci. Rev. 58, 121–142.

Peacock, D.C.P., Sanderson, D.J., 1991. Displacements, segment linkage and relay ramps in normal fault zones. J. Struct. Geol. 13, 721–733.

Peacock, D.C.P., Sanderson, D.J., 1994. Geometry and development of relay ramps in normal fault systems. Bull. Am. Assoc. Pet. Geol. 78, 147–165.

Peiro, A., Simón, J.L., Liesa, C.L., 2017. New evidence of recent fracturing at the relay zone between the Concud and Teruel faults (eastern Iberian Chain). Geogaceta 62, 31–34.

Peiro, A., Simón, J.L., Román-Berdiel, T., 2019. Zonas de relevo de falla en el margen oriental de la Fosa del Jiloca (Cordillera Ibérica): geometría, cinemática y modelización analógica. Bol. Geol. Min. 3. (in press).

Peña, J.L., 1981. Las acumulaciones cuaternarias de la confluencia de los ríos Alfambra y Guadalaviar, en las cercanías de Teruel. Actas VII Coloquio de Geografía, Pamplona, pp. 255–259.

Peña, J.L., Gutiérrez, M., Ibáñez, M.J., Lozano, M.V., Rodríguez, J., Sánchez, M., Simón, J.L., Soriano, M.A., Yetano, L.M., 1984. Geomorfología de la provincia de Teruel. Instituto de Estudios Turolenses, Teruel.

Ramberg, H., 1981. Gravity, Deformation and the Earth's Crust in Theory, Experiments and Geological Applications. Academic Press, London.

Ramírez, J.I., Olivé, A., Moissenet, E., Aragonés, E., Ramírez, J., Leal, M.C., Aguilar, M.J., Adrover, R., Giner, J., Gutiérrez, J.C., Goy, A., Comas, M.J., Portero, J.M., Gabaldón, V., 1983. Mapa Geológico de España 1: 50.000. Instituto Geológico y Minero, Madrid. hoja 541 (Santa Eulalia).

Ramsay, J.G., Huber, M.I., 1987. The Techniques of Modern Structural Geology, Vol. 2: Folds and Fractures. Academic Press, London, pp. 309–700.

Roca, E., Guimerá, J., 1992. The Neogene structure of the eastern Iberian margin: structural constraints on the crustal evolution of the Valencia trough (western Mediterranean). Tectonophysics 203, 203–218.

Román-Berdiel, T., Casas, A.M., Pueyo, E.L., Peiro, A., Soto, R., Pohlenz, A., Warsitzka, M., Rosenau, M., 2019. Ring Shear Test Data of Quartz Sand and Colored Quartz Sand Used for Analogue Experiments in the Analogue Modelling Laboratory of the University of Zaragoza. GFZ Data Services. Spain (EPOS TNA call 2017). doi:10.5880/fidgeo.2019.025.

Rotevatn, A., Fossen, H., Hesthammer, J., 2007. Are relay ramps conduits for fluid flow? Structural analysis of a relay ramp in Arches National Park, Utah. Geological Society of London 270, 55–71. Special Publications.

Rubio, J.C., Simón, J.L., 2007. Tectonic subsidence vs. Erosional lowering in a controversial intramontane depression: the Jiloca Basin (Iberian Chain, Spain). Geol. Mag. 144, 1–15.

Rudolf, M., Boutelier, D., Rosenau, M., Schreurs, G., Oncken, O., 2016. Rheological benchmark of silicone oils used for analog modeling of short- and long-term lithospheric deformation. Tectonophysics 684, 12–22.

Sánchez Fabre, M., 1989. Estudio geomorfológico de la Depresión de Alfambra-Teruel-Landete y sus rebordes montañosos Ph.D. thesis. Universidad de Zaragoza.

Schellart, W.P., 2000. Shear test results for cohesion and friction coefficients for different granular materials: scaling implications for their usage in analogue modelling. Tectonophysics 324, 1–16.

Simón, J.L., 1982. Compresión y distensión alpinas en la Cadena Ibérica Oriental Ph.D. thesis. Universidad de Zaragoza.

Simón, J.L., 1983. Tectónica y neotectónica del sistema de fosas de Teruel. Teruel 69, 21–97.

Simón, J.L., 1989. Late cenozoic stress field and fracturing in the iberian Chain and ebro basin (Spain). J. Struct. Geol. 11, 285–294.

Simón, J.L., Arlegui, L., Liesa, C.L., 2008. Stress partioning: a practical concept for analysing boundary conditions of brittle deformation. Geodin. Acta 53, 1057–1065.

Simón, J.L., Arlegui, L., Lafuente, P., Liesa, C.L., 2012. Active extensional faults in the central-eastern Iberian Chain, Spain. J. Iber. Geol. 38, 127–144.

Simón, J.L., Arlegui, L.E., Ezquerro, L., Lafuente, P., Liesa, C.L., Luzón, A., 2016. Enhaced paleoseismic succession at the Concud Fault (Iberian Chain, Spain): new insights for seismic hazard assessment. Nat. Hazards 80, 1967–1993.

Simón, J.L., Arlegui, L.E., Ezquerro, L., Lafuente, P., Liesa, C.L., Luzón, A., 2017. Structure and paleoseismology of the Teruel fault: dynamic interaction and strain partitioning with the Concud fault (eastern iberian Chain, Spain). J. Struct. Geol. 103, 100–119.

Simón, J.L., Serón, F.J., Casas, A.M., 1988. Stress deflection and fracture development in a multidirectional extension regime. Mathematical and experimental approach with field examples. Ann. Tect. 2, 21–32.

Trudgill, B., Cartwright, J., 1994. Relay-ramp forms and normal-fault linkages, canyonlands national park, Utah. Bull. Geol. Soc. Am. 106, 1143–1157.

Walsh, J.J., Watterson, J., 1991. Geometric and kinematic coherence and scale effects in normal fault systems. In: Roberts, A.M., Yielding, G., Freeman, B. (Eds.), The Geometry of Normal Faults. Geological Society Special Publication, pp. 193–203. No 56.

Walsh, J.J., Watterson, J., Bailey, W.R., Childs, C., 1999. Fault relays, bends and branch-lines. J. Struct. Geol. 21, 1019–1026.

Weijermars, R., Schmeling, H., 1986. Scaling of Newtonian and non-Newtonian fluid dynamics without inertia for quantitative modelling of rock flow due to gravity (including the concept of rheological similarity). Phys. Earth Planet. Inter. 43, 316–330.

Willemse, E.J.M., 1997. Segmented normal faults: correspondence between three-dimensional mechanical models and field data. J. Geophys. Res. 1902, 675–692.

Younes, A.I., McClay, K.R., 2002. Development of accommodation zones in the gulf of suez-red sea rift, Egypt. AAPG (Am. Assoc. Pet. Geol.) Bull. 86, 1007–1010.

Young, M.J., Gawthorpe, R.L., Hardy, S., 2001. Growth and linkage of a segmented normal fault zone; the late jurassic murchison-statfjord north fault, northern north sea. J. Struct. Geol. 23, 1933–1952.

Footnotes

Text Footnotes

[1] Roca and Guimerà, 1992

[2] Rudolf et al., 2016

[3] Instead of a "y" there should be an "and"

Queries and Answers

Query: Your article is registered as a regular item and is being processed for inclusion in a regular issue of the journal. If this is NOT correct and your article belongs to a Special Issue/Collection please contact s.sankaran@elsevier.com immediately prior to returning your corrections.

Answer: It does not belong to any Special Issue/Collection, it is for a regular issue of the journal.

Query: Please confirm that given names and surnames have been identified correctly and are presented in the desired order and please carefully verify the spelling of all authors' names.

Answer: Yes

Query: Please confirm that the provided email “apeiro@unizar.es” is the correct address for official communication, else provide an alternate e-mail address to replace the existing one, because private e-mail addresses should not be used in articles as the address for communication.

Answer: The provided email “apeiro@unizar.es” is the correct address for official communication.

Query: The citation(s) 'Ferril and Morris, 2001, Cartwright et al., 1995; Roca and Guimerà, 1992, Román-Berdiel et al., 2018, Panien et a., 2006, Rudolf et al. 2016' has been changed to match the author name/date in the reference list. Please check here and in subsequent occurrences.

Answer: Changes of references "Ferril and Morris, 2001; Cartwright et al., 1995; Román-Berdiel et al., 2018 and Panien et a., 2006" are correct and accepted.

But "Roca and Guimerà, 1992" is the correct reference, so it must be changed in the list.

And "Rudolf et al. 2016" has been changed for "RudolfBoutelier et al., 2016" and is incorrect, the correct form would be "Rudolf et al., 2016"

Query: Have we correctly interpreted the following funding source(s) and country names you cited in your article: Geotransfer-E32_17R, FEDER, Spain?

Answer: The funding sources are the Gobierno de Aragón and the Programa Operativo FEDER Aragón 2014–2020, both from our country Spain. And the grant number is Geotransfer-E32_17R.